Chapter 3

Nonlinear, Dispersive Long Waves in Water of Variable Depth

James T. Kirby

Center for Applied Coastal Research
University of Delaware, Newark, DE 19716, USA

Abstract

The use of weakly-dispersive models to compute the propagation of nonlinear ocean surface waves in the coastal environment is reviewed. Models which are fully two-dimensional in horizontal coordinates are discussed first, and various approximations involved in various models are developed and compared. Available tests of the accuracy of model predictions are also reviewed. Attempts to incorporate realistic effects including wave breaking, shoreline runup and wave-current interaction into model schemes are discussed. Subsequently, models for one-directional and weakly-two-directional propagation are briefly reviewed. Finally, frequency-domain formulations are reviewed. In all cases, the primary concentration is on aspects of model development related to the computation of realistic waves in the ocean environment.

1 Introduction

Water waves in shallow water (characterized by depths which are small compared to a wavelength) deviate more severely from the basic assumptions of linear wave theory than do waves in deeper water. Waves in shallow water are modified rapidly over distances comparable to a wavelength, due to weak frequency dispersion and, as a result, nearly resonant interaction between sets of three Fourier harmonics. These resonant interactions lead to a strong transfer of energy from fundamental to higher harmonic components as waves approach shore over natural beaches,

leading to waves having relatively narrow crests and broad troughs. In addition, the rapid transfer of energy from low to high frequencies is manifested in front-to-back asymmetry of the wave profile as the wave pitches towards the shore. Finally, difference interactions lead to a rapid growth in low-frequency energy as well, leading to shore-normal surf beat or longshore propagating edge wave and leaky mode components.

Linear theory does not give us much of a route to describing the complexity of wave motion in the final stages of shoaling or in the surf zone. For this reason, a body of theory and computational techniques has developed over the years that is specifically aimed at describing the regime where frequency dispersion effects are small and nonlinearity takes on an equal or more important role. The first steps in the study of these phenomena were made by Airy [1], who obtained the Nonlinear Shallow Water (NSW) equations governing nondispersive, nonlinear wave propagation, and by Boussinesq [2] and Korteweg and deVries [3], who provided models incorporating the leading order effect of frequency dispersion in the long wave approximation. This body of work has played a central role in the evolution of the mathematical physics of waves that exhibit a balance between nonlinear and dispersion effects. In particular, the Korteweg-deVries (KdV) equation has been proposed as the principle model equation for a wide range of physical phenomena, and has generated a vast body of literature related to its exact solution for arbitrary initial conditions by means of the Inverse Scattering Transform [4] [5]. Many textbook treatments of this basic aspect of the theory for waves in an infinite or periodic domain now exist [6] [7].

In the open coastal environment, the physical distance traversed by a surface wind wave propagating from the point where it begins to be significantly affected by the bottom until it reaches shore is often no more than several wavelengths. Thus, the problem of computing the evolution of waves through domains with significant inhomogeneities (occuring over length scales which are not terribly long compared to a wavelength) is of central importance. The problem of rapid wave evolution in a varying domain is different from the more academic problem of evolution over long distance in a uniform domain, and remains more a problem for numerical analysis. It is this aspect of the theory for weakly-dispersive long waves that is primarily reviewed here.

The modern birth of the study of nonlinear wave propagation over an uneven bottom took place in the late 1960's [8] [9] [10]. Peregrine [9]

provided the derivation of a Boussinesq-type model using depth-averaged velocity as the dependent variable, and provided the first numerical calculations of the phenomenon of nonlinear wave shoaling and evolution. Development of these techniques continued through the 1970's and 80's [11] [12] [13], but awaited the development of both theoretical techniques for extending the range of applicability of the models (through improved linear dispersion properties), as well as the development and availability of computers capable of making model computations on a more routine basis. Both of these hurdles have been crossed, and there has been a resulting explosion of interest in shallow water wave models in the past ten years.

In this review, we first concentrate on the development of the Boussinesq model framework, and review recent advances which have extended the applicability of these models over much of the range of depths where waves feel the bottom. Efforts to extend the Boussinesq model approach to cover wave breaking, shoreline runup and wave-current interaction are also reviewed. Recent results in the area of reduced-dimension, forward-propagation models are also considered, and we finish with a discusson of spectral approaches to wave computations.

2 Governing equations and scaling fundamentals

We concentrate here on a review of the development of models for the propagation of waves through a homogeneous inviscid fluid with density ρ. We employ a Cartesian coordinate system with z oriented upward and with the x, y plane lying in the plane of the still water free surface. The fluid is bounded below by a surface $F_b = z + h(x, y, t) = 0$ and above by a surface $F_s = z - \eta(x, y, t) = 0$. Time dependence in the surface is an obvious manifestation of wave motion. We allow for time dependence in the bottom bounding surface to allow for the possibility of tsunami genesis through earthquake motions and other shifts in bottom geometry.

In section 2.4, we will introduce scaling assumptions that make a strong distinction between the relative size of horizontal and vertical motions. For now, we retain a more general formulation. Introducing a velocity vector $\boldsymbol{u}$ given by

$$\boldsymbol{u} = (u(\mathbf{x}, z, t), v(\mathbf{x}, z, t), w(\mathbf{x}, z, t)), \tag{1}$$

where $\mathbf{x} = (x, y)$ is the position vector in the horizontal propagation space, we may write the governing equations as

$$\nabla_3 \cdot \boldsymbol{u} = 0 \tag{2}$$

$$\boldsymbol{u}_t + \boldsymbol{u} \cdot \nabla_3 \boldsymbol{u} + \frac{1}{\rho} \nabla_3 p + g \mathbf{i}_z = 0, \tag{3}$$

where ∇_3 denotes a gradient in three dimensions. We will often make a distinction between horizontal and vertical velocity components. We define the horizontal velocity

$$\mathbf{u} = (u(\mathbf{x}, z, t), v(\mathbf{x}, z, t)) \tag{4}$$

and denote a gradient in horizontal coordinates by ∇. Kinematic constraints on the bounding upper and lower surfaces lead to the conditions

$$\eta_t + \mathbf{u} \cdot \nabla \eta = w; \qquad z = \eta(\mathbf{x}, t) \tag{5}$$

and

$$h_t + \mathbf{u} \cdot \nabla h = -w; \qquad z = -h(\mathbf{x}, t) \tag{6}$$

Finally, we ignore dynamic interaction with an overlying air layer and simply specify that pressure be constant on the upper bounding surface,

$$p = 0; \qquad z = \eta(\mathbf{x}, t). \tag{7}$$

2.1 Irrotational flow

The formulation above is completely adequate for the general problem of inviscid, incompressible flow. Several of the formulations considered below will rest only on the formulation above, without recourse to further assumptions. However, due to the implications of Kelvin's theorem for inviscid, barotropic fluids, waves are often assumed to fall into the category of irrotational flows; i.e., flows having no vorticity or circulation. In this case, stronger conditions may be imposed on the formulation of the wave motion problem. For the case of irrotational motion,

$$\nabla_3 \times \boldsymbol{u} = 0 \tag{8}$$

we may introduce a velocity potential $\phi(\mathbf{x}, z, t)$ such that

$$\boldsymbol{u} = \nabla_3 \phi. \tag{9}$$

Subsequent use of (9) in (2) then gives

$$\nabla_3^2 \phi = 0, \tag{10}$$

which is Laplace's equation for the velocity potential. This result is supplemented by the first integral of the Euler equation (3), known as Bernoulli's equation,

$$\frac{p}{\rho} + \phi_t + gz + \frac{1}{2}|\nabla_3 \phi|^2 = C(t), \tag{11}$$

which relates the pressure field to the velocity field. Evaluating (11) at the free surface and introducing the constraint (7) leads to a dynamic free surface boundary condition

$$g\eta + \phi_t + \frac{1}{2}|\nabla_3 \phi|^2 = 0, \tag{12}$$

where the Bernoulli constant is absorbed under the assumption that the free surface coincides with the level surface $z = 0$ when no wave activity or current field is present. Finally, the kinematic boundary conditions are given by

$$\eta_t + \nabla\phi \cdot \nabla\eta = \phi_z \quad ; \qquad z = \eta \tag{13}$$

$$\nabla\phi \cdot \nabla h = -\phi_z \quad ; \qquad z = -h. \tag{14}$$

2.2 Variational formulation

The existence of a Lagrangian for irrotational free surface flows was introduced originally by Luke [14], who showed that the Lagrangian was given by the integral of fluid pressure over the depth; i.e.,

$$\mathcal{L}(\mathbf{x}, t) = \int_{-h}^{\eta} p(\mathbf{x}, z, t) dz. \tag{15}$$

Using Bernoulli's equation (11) above, we may recast $\mathcal{L}$ in the form

$$\mathcal{L}(\mathbf{x}, t) = \frac{1}{2}\rho g h^2 - \rho \int_{-h}^{\eta} \phi_t dz - \left[\frac{1}{2}\rho g \eta^2 + \frac{\rho}{2}\int_{-h}^{\eta} [(\nabla\phi)^2 + (\phi_z)^2] dz\right]. \tag{16}$$

Luke's principle then states that the integral of $\mathcal{L}$ over all horizontal space and time is then stationary with respect to variations in η and ϕ

$$\delta \int_{\mathbf{x}} \int_t \mathcal{L}(\mathbf{x}, t; \eta, \phi) d\mathbf{x} dt = 0, \tag{17}$$

where we neglect the influence of lateral boundaries on the specification of the problem. It may be shown [14] that this formulation is equivalent to the boundary value problem specified by equations (10 - 14). An examination of (16) shows that the first term is trivial, as it does not depend on a dynamic variable. The last term in brackets consists of the sum of the potential energy per unit area in the horizontal plane $\mathcal{V}$ and the kinetic energy per unit area in the horizontal plane $\mathcal{T}$. We denote the sum of these two energies as the total energy $\mathcal{H}(\mathbf{x}, t)$. The Lagrangian (16) is fully equivalent to the usual Lagrangian from classical mechanics,

$$\mathcal{L} = \mathcal{T} - \mathcal{V}. \tag{18}$$

This result may be established by use of Green's first identity and Laplace's equation applied to the kinetic energy integral in (16). Following Miles [15], we may integrate the second term in (16) by parts once and obtain the relation

$$\int_{-h}^{\eta} \phi_t dz = \frac{\partial}{\partial t} \int_{-h}^{\eta} \phi dz - \xi(\mathbf{x}, t)\eta_t; \qquad \xi(\mathbf{x}, t) = \phi(\mathbf{x}, z = \eta, t), \tag{19}$$

where the first term integrates to the boundaries in time in (17) and hence has no dynamic significance. The Lagrangian may then be written as

$$\mathcal{L} = \rho\xi\eta_t - \mathcal{H}. \tag{20}$$

This result may be further identified as the Legendre transform [16], with $\mathcal{H}$ denoting the Hamiltonian, η the canonical coordinate, and $\rho\xi$ the conjugate momentum. Proof that the surface wave problem for irrotational motion is a Hamiltonian system was provided originally by Zakharov [17].

2.3 Computational approaches using the full equations

Given the full boundary value problem for fluid motion, it is possible to construct numerical solutions for the full three-dimensional problem. This approach has been pursued by a number of authors, principally using a technique known as the Volume of Fluid (VOF method). This method has been applied to both shoaling waves and breaking waves with some success [18]. Alternately, for the irrotational problem, several approaches exist which reduce the dimensionality of the problem being studied by one. Two such approaches are reviewed here.

2.3.1 Hamiltonian canonical evolution equations

The existence of a Hamiltonian for an irrotational flow with a free surface provides an immediate path to developing evolution equations for wave motion, in the form of the canonical equations for the evolution in time of the coordinate and conjugate momentum,

$$\eta_t = \frac{\delta \mathcal{H}}{\delta \xi}(\eta, \xi) \tag{21}$$

$$\xi_t = -\frac{\delta \mathcal{H}}{\delta \eta}(\eta, \xi), \tag{22}$$

where the derivatives are functional derivatives with respect to the dependent variables. Following Miles [15], (21) and (22) may be written as

$$\eta_t = -\nabla\xi \cdot \nabla\eta + \zeta(1 + \nabla\eta \cdot \nabla\eta) \tag{23}$$

$$\xi_t = -g\eta - \frac{1}{2}\nabla\xi \cdot \nabla\xi + \frac{1}{2}\zeta^2(1 + \nabla\eta \cdot \nabla\eta), \tag{24}$$

where $\zeta = \phi_z(\mathbf{x}, z = \eta, t)$ is the vertical velocity at the surface. Equations (23) and (24) can be solved if an associated solution of Laplace's equation is used to obtain the vertical velocity. Examples of successful direct approaches using this problem formulation may be found in [19], [20]. These approaches often utilize methods such as Fourier transforms to obtain solutions to Laplace's equation efficiently. They are thus usually restricted to periodic domains and are difficult to apply to the general coastal wave propagation problem.

Alternately, Radder [21] has suggested an approach in which the Hamiltonian evolution equations are written in terms of η and the stream function at the free surface,which is evaluated after conformally mapping the fluid domain into a strip. Due to the transformation method utilized, the method is not immediately applicable to wave propagation in two horizontal directions. Otta & Dingemans [22] show a method for computing solutions of Radder's model utilizing sinc-series to discretize the remaining Fourier integral. They further use a check on the approach to singularity of the Jacobian of the transformation from physical to mapped space as a test for breaking, and modify the surface and stream function evolution subsequent to the break point to model the effect of wave breaking, with reasonable success.

Use of Hamilton's principle to construct evolution equations in the long wave setting usually proceeds along slightly different lines, and we defer a discussion of this aspect until Section 4.

2.3.2 Boundary integral equations.

An alternate approach to the inviscid irrotational flow problem results from the fact that Laplace's equation for the fluid interior may be converted to an integral equation on the surface bounding the fluid domain. Denoting the boundary by Γ, which is either a closed contour in the case of flow in one horizontal coordinate and z, or a closed surface in the fully three-dimensional case, we may write an equation for the value of the potential at a point on the boundary surface as

$$\phi(\boldsymbol{x}_l) = \int_\Gamma \left[\phi_{\mathbf{n}}(\boldsymbol{x})G(\boldsymbol{x},\boldsymbol{x}_l) - \phi(\boldsymbol{x})G_{\mathbf{n}}(\boldsymbol{x},\boldsymbol{x}_l)\right] d\Gamma(\boldsymbol{x}), \tag{25}$$

where G is the free-space Green function and where subscript $\mathbf{n}$ denotes a derivative in the direction of the outward normal vector. Several different approaches exist for solving (25) together with the surface boundary conditions. Grilli and coworkers [23] [24] use the dynamic surface boundary condition (12) together with a kinematic condition

$$D\boldsymbol{x} = \nabla_3\phi; \qquad D() = ()_t + \nabla_3 \cdot \nabla_3() \tag{26}$$

to step the solution forward in time and update the position of the boundary, after which (25) is used to update the velocity field. Applications of this model have been limited to date to two-dimensional problems in the vertical plane. Grilli *et al* [25] have compared numerical calculations of solitary waves shoaling on a plane beach to laboratory data, and have found that the model predicts the actual wave motion to within the accuracy of the available data.

Several researchers have implemented similar approaches using this modelling technique [26] [27] [28] [29]. Fully three-dimensional applications of the technique are typically based on panel methods [30] [31] and are still relatively scarce.

2.4 Scaling of dimensional variables

Development of approximate formulations for long wave motion in a layer of water usually rests on the identification of two scaling parameters; a

water depth to wavelength ratio (denoted here by μ), and a wave height to water depth ratio (denoted here by ϵ). An alternate nonlinear parameter can be obtained by multiplying μ and ϵ to obtain the ratio of wave height to wave length, the so-called wave steepness.

Following [32], we use a reference wavenumber k_0 to scale horizontal distances x, y, a reference water depth h_0 to scale the vertical coordinate z and local depth $h(x, y)$, and amplitude a to scale the surface displacement η. We then introduce the parameters $\delta = a/h_0$ and $\mu^2 = (k_0 h_0)^2$. Based on these, we choose a scale of $(k_0(gh_0)^{1/2})^{-1}$ for time t and $\delta h_0 (gh_0)^{1/2}/\mu$ for velocity potential ϕ. Introducing these scales into the boundary value problem for inviscid, irrotational motion leads to the problem

$$\phi_{zz} + \mu^2 \nabla^2 \phi = 0; \qquad -h \le z \le \delta\eta \tag{27}$$

$$\phi_z + \mu^2 \nabla h \cdot \nabla \phi = 0; \qquad z = -h \tag{28}$$

$$\eta + \phi_t + \frac{\delta}{2}[(\nabla\phi)^2 + \frac{1}{\mu^2}(\phi_z)^2] = 0; \qquad z = \delta\eta \tag{29}$$

$$\eta_t + \delta \nabla\phi \cdot \nabla\eta - \frac{1}{\mu^2}\phi_z = 0; \qquad z = \delta\eta. \tag{30}$$

We develop an equation expressing volume flux conservation by integrating (27) over z from $-h$ to $\delta\eta$ and using (28) and (30) to obtain

$$\eta_t + \nabla \cdot \mathbf{M} = 0; \qquad \mathbf{M} = \int_{-h}^{\delta\eta} \nabla\phi dz. \tag{31}$$

In the following, we use (31) to obtain expressions for mass conservation, while a momentum equation is obtained using the Bernoulli equation (29). Choice of representative length and time scales for the propagation of irregular waves in a variable-depth region is problematic, since waves satisfying some scaling argument or restriction in one portion of the domain are almost certain to violate these conditions in another portion of the domain. We proceed here with a standard construction of the dimensionless formulation. We will address the effect of violating the basic scaling assumptions as a separate issue later.

2.5 An aside on nomenclature

Approximate models for wave propagation are obtained through a number of routes, and confusion may arise if there is not a precise understanding of how the name of a result is tied to the method for obtaining that result. The rules followed below are thus outlined here.

Most of the models discussed below are related to a description of the flow field based on a series solution of Laplace's equation retaining terms to $O(\mu^2)$, which gives a vertical distribution of horizontal velocity (at least over a flat bottom) that is quadratic in z or some related vertical coordinate. The corresponding vertical distribution of vertical velocity is linear in z. A quick check of the approximate expressions for the velocity potential used below shows that the expression for the fluid vorticity is identically zero to $O(\mu^2)$, and thus the flow fields are irrotational to the order of the approximation. We will refer to any model based on a potential as a starting point, or on an assumption of the form of the internal kinematics that would correspond to the use of a potential, as a *Boussinesq-type*, or in short, a *Boussinesq* model. Since the specification of canonical variables in the Hamiltonian formulation uses a velocity potential, approximate models obtained using this approach fall in this category as well.

In contrast, there are a number of models that assume *a priori* that the fluid moves in vertical columns which remain vertical and are at most stretched by up and down motion of the surface. This assumption has been used in a number of models, including models based on approximation of the governing Euler equations (Serre [33], Su & Gardner [34]) or satisfaction of global mass, momentum and energy constraints (Green & Naghdi [35]). These models are variously referred to as Serre equations or GN equations, and we will show below that they are in fact the same, at least at the leading order of approximation used in constructing them.

Finally, we will make a distinction between *fully-nonlinear* and *weakly-nonlinear* models. We will refer to a model as being *fully-nonlinear* if the known information about the internal flow field is used to satisfy the surface boundary conditions imposed at the free surface, with the only truncation allowed being used to maintain consistency in the ordering with respect to the parameter μ^2. In this context, the usual Airy or Nonlinear Shallow Water (NSW) equations would be the appropriate fully-nonlinear equations in the limit $\mu^2 \to 0$. Any model which invokes a further restriction on nonlinearity by fixing a relation between the parameters δ and μ^2 in a regime where $\mu^2 \ll 1$ will be referred to as being weakly-nonlinear.

3 Derivation of Boussinesq equations

The basic problem of water wave propagation is two-dimensional in the horizontal coordinates $\mathbf{x} = (x, y)$, and we will start with models that provide a full treatment of arbitrary motions in this coordinate system.

The central goals in the derivation of an approximate wave propagation model in free surface hydrodynamics are to:

1. obtain an approximation for the dependence of the solution on the vertical coordinate z.

2. eliminate the cross-space z in favour of a model in the propagation space x, y, t.

In the case of Boussinesq models, the representation of the vertical dependence of the solution as a low-order polynomial leads to a recursion relation in which higher order coefficients in the series are determined by the spatial variation of the lowest order coefficient. The choice of this coefficient then specifies the dependent variable. This choice is non-unique, and thus there will be a family of models satisfying a given set of scaling restrictions, rather than one fixed, unique Boussinesq model. Mathematicians have typically played down the importance of the distinctions between the members of this family, tending to lump them together as representations of a given asymptotic regime. However, as will be seen below, the various forms of the model equations can have significantly different properties (particularly in terms of linear dispersion characteristics) when applied in water depths which are large relative to the asymptotic range of validity. For this reason, modellers are quite interested in the differences in behaviour of the various members of the asymptotically-equivalent family. Witting [36] pointed out that it is possible to construct weakly-dispersive models that are characterized by dispersion relations having the form of rational polynomial or Padé approximants, and that are numerically far more accurate as the depth becomes relatively large. We illustrate the consistant construction of such a model below, following an approach developed by Nwogu [37]. Other means for obtaining models with extended accuracy in their dispersion relations include direct manipulation of highest-order (dispersive) terms in an existing set of governing equations [38] [39], or the use of an alternate vertical shape function in order to introduce correct dispersion properties at some reference frequency [40] [41].

The derivation of the Boussinesq equations illustrated here proceeds by obtaining an approximate solution to the Laplace equation in the fluid interior and then using the resulting information in the dynamic surface boundary condition (29) and the depth integrated continuity equation (31). As pointed out by Mei [32], the resulting derivation does not require any *a priori* assumption about the size of δ; all information provided by (29) and (31) can be retained. The resulting fully-nonlinear equations will depend on the level of accuracy retained in the approximation of ϕ. Weakly-nonlinear Boussinesq equations are then obtained by invoking the restriction $\delta = O(\mu^2)$.

3.1 Approximate expressions for the velocity potential

The Boussinesq-type equations may be obtained by introducing a series expansion for ϕ of the form

$$\phi(\mathbf{x}, z, t) = \sum_{n=0}^{\infty} (h+z)^n \phi_n(\mathbf{x}, t). \tag{32}$$

An expression for ϕ which retains terms to $O(\mu^2)$ and satisfies the bottom boundary condition is given by

$$\phi = \phi_0(\mathbf{x}, t) - \mu^2 (h+z) \nabla h \cdot \nabla \phi_0 - \mu^2 \frac{(h+z)^2}{2} \nabla^2 \phi_0 + O(\mu^4), \tag{33}$$

where ϕ_0 is the value of the velocity potential at $z = -h$. Various forms of the evolution equations are obtained by replacing ϕ_0 by the value of the potential at any level in the water column, or by the integral over the depth. Any choice will lead to a set of model equations with the same level of asymptotic approximation but with numerically different dispersion properties, as discussed below. As a first example, we will use a depth-averaged value of the potential and a related depth-averaged velocity, following Wu [42] and Mei [32]. We define the depth-averaged potential according to

$$\bar{\phi}(\mathbf{x}, t) = \frac{1}{H} \int_{-h}^{\eta} \phi(\mathbf{x}, z, t) dz, \tag{34}$$

where $H = (h + \delta\eta)$ is the total local water depth. Using (33) in (34) gives

$$\bar{\phi} = \phi_0 - \mu^2 \left(\frac{H}{2} \nabla h \cdot \nabla \phi_0 + \frac{H^2}{6} \nabla^2 \phi_0 \right). \tag{35}$$

This expression is then used in (33) to obtain an expression for ϕ in terms of $\bar{\phi}$:

$$\phi = \bar{\phi} + \frac{\mu^2}{2}(H - 2(h+z))\nabla h \cdot \nabla\bar{\phi} + \frac{\mu^2}{6}(H^2 - 3(h+z)^2)\nabla^2\bar{\phi} + O(\mu^4). \quad (36)$$

Alternately, following Wei *et al* [43] and Chen & Liu [44], we denote ϕ_α as the value of ϕ at a reference elevation $z = z_\alpha(\mathbf{x})$, or

$$\phi_\alpha = \phi_0 - \mu^2(h + z_\alpha)\nabla h \cdot \nabla\phi_0 - \mu^2\frac{(h+z_\alpha)^2}{2}\nabla^2\phi_0 + O(\mu^4). \quad (37)$$

This expression is then used in (33) to obtain an expression for ϕ in terms of ϕ_α:

$$\phi = \phi_\alpha + \mu^2(z_\alpha - z)\nabla\cdot(h\nabla\phi_\alpha) + \frac{1}{2}\mu^2(z_\alpha^2 - z^2)\nabla^2\phi_\alpha + O(\mu^4). \quad (38)$$

3.2 Model based on depth-integrated potential or velocity

3.2.1 Two-equation model for η and $\bar{\phi}$

Wu [42] was one of the first to point out that a two-equation model for η and the chosen dependent variable representing the potential appeared to be a good candidate for computational work, since it reduces the number of equations and dependent variables by one compared to a formulation involving η and a horizontal velocity vector. Wu formulated a model in the standard Boussinesq approximation, including the effects of applied surface pressure and moving bottom. We illustrate the derivation of his model here and provide a fully-nonlinear version as an intermediate step.

Using (35) in (31) to obtain an expression for volume flux $\mathbf{M}$ gives

$$\begin{aligned}\mathbf{M} &= H\left[\nabla\bar{\phi} + \mu^2\left\{\frac{1}{2}(\nabla H - 2\nabla h)\nabla h\cdot\nabla\bar{\phi}\right.\right.\\ &\quad \left.\left. + \frac{1}{6}H(2\nabla H - 3\nabla h)\nabla^2\bar{\phi}\right\}\right] + O(\mu^4). \quad (39)\end{aligned}$$

The expression goes to zero identically as the total depth H goes to zero, which serves as a natural shoreline boundary condition. The corresponding form of the Bernoulli equation (29) is

$$\eta + \bar{\phi}_t + \frac{\delta}{2}(\nabla\bar{\phi}\cdot\nabla\bar{\phi}) - \mu^2 H\left[\frac{1}{2}D(\nabla h\cdot\nabla\bar{\phi}) + \frac{H}{3}D(\nabla^2\bar{\phi})\right]$$

$$+\frac{\delta\mu^2}{6}\left[H^2(\nabla^2\bar{\phi})^2 - 3H(\nabla h\cdot\nabla\bar{\phi})\nabla^2\bar{\phi} - 3(\nabla h\cdot\nabla\bar{\phi})^2\right] = O(\mu^4), \quad (40)$$

where the operator $D() = ()_t + \delta\nabla\bar{\phi}\cdot\nabla()$. The usual Boussinesq approximation is recovered by retaining terms of $O(\delta,\mu^2)$ which gives the set of equations

$$\mathbf{M} = H\nabla\bar{\phi} - \mu^2\nabla h\left\{\frac{h}{2}\nabla\cdot(h\nabla\bar{\phi}) - \frac{h^2}{3}\nabla^2\bar{\phi}\right\} + O(\delta^2,\delta\mu^2,\mu^4) \quad (41)$$

and

$$\eta+\bar{\phi}_t+\frac{\delta}{2}(\nabla\bar{\phi}\cdot\nabla\bar{\phi})-\mu^2\left[\frac{h}{2}\nabla\cdot(h\nabla\bar{\phi}_t) - \frac{h^2}{6}\nabla^2\bar{\phi}_t\right] = O(\delta^2,\delta\mu^2,\mu^4). \quad (42)$$

Equations (41) and (42) are identical to the results given by Wu [42] after neglecting pressure forcing and bottom motion.

3.2.2 Three-equation model for η and $\overline{\mathbf{u}}$

A model based on the depth-averaged horizontal velocity is obtained next. The velocity $\overline{\mathbf{u}}$ is defined by

$$\begin{aligned}\overline{\mathbf{u}} &= \frac{1}{H}\int_{-h}^{\delta\eta}\nabla\phi dz \quad (43)\\ &= \nabla\bar{\phi} + \frac{\mu^2}{2}(\nabla H - 2\nabla h)(\nabla h\cdot\nabla\bar{\phi}) + \frac{\mu^2}{6}(2\nabla H - 3\nabla h)\nabla^2\bar{\phi} + O(\mu^4).\end{aligned}$$

Using (43) in the expression (39) for the mass flux gives

$$\mathbf{M} = H\overline{\mathbf{u}} + O(\mu^4), \quad (44)$$

which in fact is accurate to all orders in μ. The corresponding momentum equation is obtained by taking the gradient of the Bernoulli equation (40), which gives

$$\begin{aligned}&\overline{\mathbf{u}}_t + \delta(\overline{\mathbf{u}}\cdot\nabla)\overline{\mathbf{u}} + \nabla\eta - \frac{\mu^2}{2}\left[(\nabla H - 2\nabla h)\nabla h\cdot\overline{\mathbf{u}}\right]_t\\ &-\frac{\mu^2}{6}\left[H(2\nabla H - 3\nabla h)\nabla\cdot\overline{\mathbf{u}}\right]_t - \mu^2\nabla\left[\frac{H}{2}D^*(\nabla h\cdot\overline{\mathbf{u}}) + \frac{H^2}{3}D^*(\nabla\cdot\overline{\mathbf{u}})\right]\\ &+\frac{\delta\mu^2}{6}\nabla\Big[H^2(\nabla\cdot\overline{\mathbf{u}})^2 - 3H(\nabla h\cdot\overline{\mathbf{u}})(\nabla\cdot\overline{\mathbf{u}}) - 3(\nabla h\cdot\overline{\mathbf{u}})^2\\ &-H(2\nabla H - 3\nabla h)\cdot\overline{\mathbf{u}}(\nabla\cdot\overline{\mathbf{u}}) - 3(\nabla H - 2\nabla h)\cdot\overline{\mathbf{u}}(\nabla h\cdot\overline{\mathbf{u}})\Big] = O(\mu^4), \quad (45)\end{aligned}$$

where $D^*() = ()_t + \delta\overline{\mathbf{u}} \cdot \nabla() = D() + O(\mu^2)$.

The weakly nonlinear Boussinesq approximation is obtained by neglecting terms of $O(\delta\mu^2)$ or higher in (45), giving (44) for the mass flux and

$$\overline{\mathbf{u}}_t + \delta(\overline{\mathbf{u}} \cdot \nabla)\overline{\mathbf{u}} + \nabla\eta - \mu^2 \left[\frac{h}{2}\nabla(\nabla \cdot (h\overline{\mathbf{u}}_t)) - \frac{h^2}{6}\nabla(\nabla \cdot \overline{\mathbf{u}}_t)\right] = O(\delta\mu^2, \mu^4) \tag{46}$$

for the momentum equations. Equation (46) was given originally by Peregrine [9]. Retaining full nonlinear effects but restricting to constant still water depth $h = h_0$ reduces (45) to

$$\begin{aligned} \overline{\mathbf{u}}_t + \delta(\overline{\mathbf{u}} \cdot \nabla)\overline{\mathbf{u}} + \nabla\eta + \frac{\mu^2}{6}\left(H^2\nabla^2\overline{\mathbf{u}}\right)_t & \\ +\mu^2\nabla\left[-\frac{\delta}{3}H^2\overline{\mathbf{u}} \cdot \nabla^2\overline{\mathbf{u}} + \frac{\delta}{2}H^2(\nabla \cdot \overline{\mathbf{u}})^2 - \frac{H^2}{2}(\nabla \cdot \overline{\mathbf{u}})_t\right] &= O(\mu^4), \end{aligned} \tag{47}$$

given by Mei [32].

3.3 Model based on potential or velocity at a fixed elevation

3.3.1 Two-equation model for η and ϕ_α

Now, we derive a two-equation model for η and ϕ_α following Wei *et al* [43]. Using (38), the expression for

M in (31) becomes

$$\begin{aligned} \mathbf{M} &= H\left[\nabla\phi_\alpha + \mu^2\left\{\nabla\left[z_\alpha\nabla \cdot (h\nabla\phi_\alpha) + \frac{z_\alpha^2}{2}\nabla^2\phi_\alpha\right]\right.\right. \\ &+ \left.\left.\frac{(h-\delta\eta)}{2}\nabla(\nabla \cdot (h\nabla\phi_\alpha)) - \frac{(h^2 - h\delta\eta + (\delta\eta)^2)}{6}\nabla^2\nabla\phi_\alpha\right\}\right] \end{aligned} \tag{48}$$

The corresponding form of the Bernoulli equation (29) becomes

$$\begin{aligned} \eta &+ \phi_{\alpha t} + \frac{\delta}{2}(\nabla\phi_\alpha)^2 + \mu^2\left[(z_\alpha - \delta\eta)\nabla \cdot (h\nabla\phi_{\alpha t}) + \frac{1}{2}(z_\alpha^2 - (\delta\eta)^2)\nabla^2\phi_{\alpha t}\right] \\ &+ \delta\mu^2\left\{\nabla\phi_\alpha \cdot [\nabla z_\alpha\nabla \cdot (h\nabla\phi_\alpha) + (z_\alpha - \delta\eta)\nabla(\nabla \cdot (h\nabla\phi_\alpha))]\right. \end{aligned}$$

$$+ \quad \nabla\phi_\alpha \cdot \left[z_\alpha \nabla z_\alpha \nabla^2 \phi_\alpha + \frac{1}{2}(z_\alpha^2 - (\delta\eta)^2)\nabla(\nabla^2\phi_\alpha) \right]$$
$$+ \quad \frac{1}{2}\left[\nabla\cdot(h\nabla\phi_\alpha)\right]^2 + \delta\eta\nabla\cdot(h\nabla\phi_\alpha)\nabla^2\phi_\alpha + \frac{1}{2}(\delta\eta)^2(\nabla^2\phi_\alpha)^2 \Big\} = 0. \quad (49)$$

Weakly-nonlinear Boussinesq equations are obtained by neglecting terms of $O(\delta\mu^2)$. The modified expression for volume flux $\mathbf{M}$ is

$$\begin{aligned} \mathbf{M} &= H\nabla\phi_\alpha + \mu^2 \left\{ h\nabla \left[z_\alpha \nabla\cdot(h\nabla\phi_\alpha) + \frac{z_\alpha^2}{2}\nabla^2\phi_\alpha \right] \right. \\ &\quad \left. + \frac{h^2}{2}\nabla(\nabla\cdot(h\nabla\phi_\alpha)) - \frac{h^3}{6}\nabla^2\nabla\phi_\alpha \right\} \end{aligned} \quad (50)$$

and the Bernoulli equation reduces to

$$\eta + \phi_{\alpha t} + \frac{\delta}{2}(\nabla\phi_\alpha)^2 + \mu^2 \left[z_\alpha \nabla\cdot(h\nabla\phi_{\alpha t}) + \frac{1}{2}z_\alpha^2\nabla^2\phi_{\alpha t} \right] = 0. \quad (51)$$

Equations (50) and (51) were given in [44]. These results are equivalent to the two-equation model (41) - (42) of Wu [42] to within rearrangements of dispersive terms.

3.3.2 Three equation model based on η and $\mathbf{u}_\alpha$

We further introduce a horizontal velocity $\mathbf{u}_\alpha$ as $\mathbf{u}_\alpha = \nabla\phi|_{z_\alpha}$. Retaining terms to $O(\mu^2)$ and to all orders in δ gives a fully nonlinear version of the model with volume flux

$$\begin{aligned} \mathbf{M} &= H\left[\mathbf{u}_\alpha + \mu^2 \left\{ \left[\frac{1}{2}z_\alpha^2 - \frac{1}{6}(h^2 - h\delta\eta + (\delta\eta)^2) \right] \nabla(\nabla\cdot\mathbf{u}_\alpha) \right. \right. \\ &\quad \left. \left. + \left[z_\alpha + \frac{1}{2}(h - \delta\eta) \right] \nabla(\nabla\cdot(h\mathbf{u}_\alpha)) \right\} \right] + O(\mu^4) \end{aligned} \quad (52)$$

and momentum equation

$$\mathbf{u}_{\alpha t} + \delta(\mathbf{u}_\alpha\cdot\nabla)\mathbf{u}_\alpha + \nabla\eta + \mu^2\mathbf{V_1} + \delta\mu^2\mathbf{V_2} = O(\mu^4), \quad (53)$$

where

$$\begin{aligned} \mathbf{V_1} &= \frac{1}{2}z_\alpha^2\nabla(\nabla\cdot\mathbf{u}_{\alpha t}) + z_\alpha\nabla(\nabla\cdot(h\mathbf{u}_{\alpha t})) \\ &\quad -\nabla\left[\frac{1}{2}(\delta\eta)^2\nabla\cdot\mathbf{u}_{\alpha t} + \delta\eta\nabla\cdot(h\mathbf{u}_{\alpha t}) \right] \\ \mathbf{V_2} &= \nabla\left[(z_\alpha - \delta\eta)(\mathbf{u}_\alpha\cdot\nabla)(\nabla\cdot(h\mathbf{u}_\alpha)) + \frac{1}{2}(z_\alpha^2 - (\delta\eta)^2)(\mathbf{u}_\alpha\cdot\nabla)(\nabla\cdot\mathbf{u}_\alpha) \right] \\ &\quad +\frac{1}{2}\nabla\left[(\nabla\cdot(h\mathbf{u}_\alpha) + \delta\eta\nabla\cdot\mathbf{u}_\alpha)^2 \right]. \end{aligned} \quad (54)$$

The weakly-nonlinear Boussinesq equations of Nwogu are recovered by neglecting terms of $O(\mu^4, \delta\mu^2)$, yielding the expressions

$$\mathbf{M} = H\mathbf{u}_\alpha + \mu^2 \left\{ \left(\frac{hz_\alpha^2}{2} - \frac{h^3}{6} \right) \nabla(\nabla \cdot \mathbf{u}_\alpha) + \left(hz_\alpha + \frac{h^2}{2} \right) \nabla(\nabla \cdot (h\mathbf{u}_\alpha)) \right\} \tag{55}$$

and

$$\mathbf{u}_{\alpha t} + \delta(\mathbf{u}_\alpha \cdot \nabla)\mathbf{u}_\alpha + \nabla\eta + \mu^2 \left\{ \frac{z_\alpha^2}{2} \nabla(\nabla \cdot \mathbf{u}_{\alpha t}) + z_\alpha \nabla[\nabla \cdot (h\mathbf{u}_{\alpha t})] \right\} = O(\delta\mu^2, \mu^4). \tag{56}$$

The fully nonlinear models derived here all have mass flux $\mathbf{M} \to 0$ at the shoreline, where $H \to 0$. This result is expected on physical grounds and appears in the nonlinear shallow water equations and in Boussinesq models where the depth-averaged velocity is the dependent variable. This condition is not automatically satisfied by Nwogu's or any weakly nonlinear Boussinesq model based on a velocity other than the depth-averaged value, making the application of these models problematic at the shoreline. All fully-nonlinear variations of any of the possible model systems should recover this condition correctly.

3.4 Choice of z_α and linearized dispersion relations

As the limitation to relatively shallow water $\mu^2 \ll 1$ is the primary factor affecting applicability of the Boussinesq models, it is important to understand the impact that the choice of dependent variables has on the implied linear dispersion relation associated with each model. To investigate this, we consider linearized forms of the model based on the depth-averaged potential (41)-(42) and the potential chosen at a fixed depth z_α, (50)-(51). For the case of one-dimensional propagation in water of constant depth $h = h_0$, the former may be written as

$$\eta_t + \bar{\phi}_{xx} = 0 \tag{57}$$

$$\bar{\phi}_t + \eta - \mu^2 \frac{1}{3} \bar{\phi}_{xxt} = 0 \tag{58}$$

and has the associated dispersion relation

$$c^2 = \frac{1}{1 + \frac{1}{3}\mu^2}, \tag{59}$$

where c is the phase speed normalized by the nondispersive phase speed $\sqrt{gh}$. Chen & Liu's model (50), (51) is written in 1-D, linearized form as

$$\eta_t + \phi_{\alpha xx} + \mu^2(\alpha + \frac{1}{3})\phi_{\alpha xxxx} = 0 \tag{60}$$

$$\phi_{\alpha t} + \eta + \mu^2\alpha\phi_{\alpha xxt} = 0 \tag{61}$$

and has the corresponding dispersion relation

$$c^2 = \frac{1 - (\alpha + \frac{1}{3})\mu^2}{1 - \alpha\mu^2}. \tag{62}$$

In (60)-(62), α is given by

$$\alpha = \frac{1}{2}\left(\frac{z_\alpha}{h}\right)^2 + \frac{z_\alpha}{h}. \tag{63}$$

The appearance of the free parameter α in (62) gives the z_α model described here (or any other extended-accuracy Boussinesq model) the ability to predict accurate phase speeds over a wide range of water depths. For example, the choice $\alpha = -1/3$ (corresponding to $z_\alpha = (1/\sqrt{3} - 1)h = -0.423h$) reproduces the relation (59) based on the depth-averaged velocity. As shown originally by Witting [36], a better result is obtained by forcing the approximate formula to coincide with the (2,2) Padé approximant, given by the choice $\alpha = -2/5$ (which, in turn, corresponds to $z_\alpha = (1/\sqrt{5} - 1)h = -0.553h$). Finally, Nwogu [37] pointed out that more accurate results can be obtained at intermediate depth by choosing α such that some measure of error is minimized. Nwogu chose to minimize the mean square error between (62) and the exact result

$$c^2 = \frac{\tanh\mu}{\mu} \tag{64}$$

over the range $0 < \omega^2 h/g < \pi$, and obtained the result

$$\alpha = -0.39; \qquad z_\alpha = -0.53h. \tag{65}$$

The dispersion relations resulting from use of the depth-averaged velocity, the Padé approximant and Nwogu's choice of α are compared to the exact result in Figure 1. Further refinements have been suggested by Chen & Liu [44], who minimized the mean square error in a combination of the phase and group velocities and obtained a slightly different value of α.

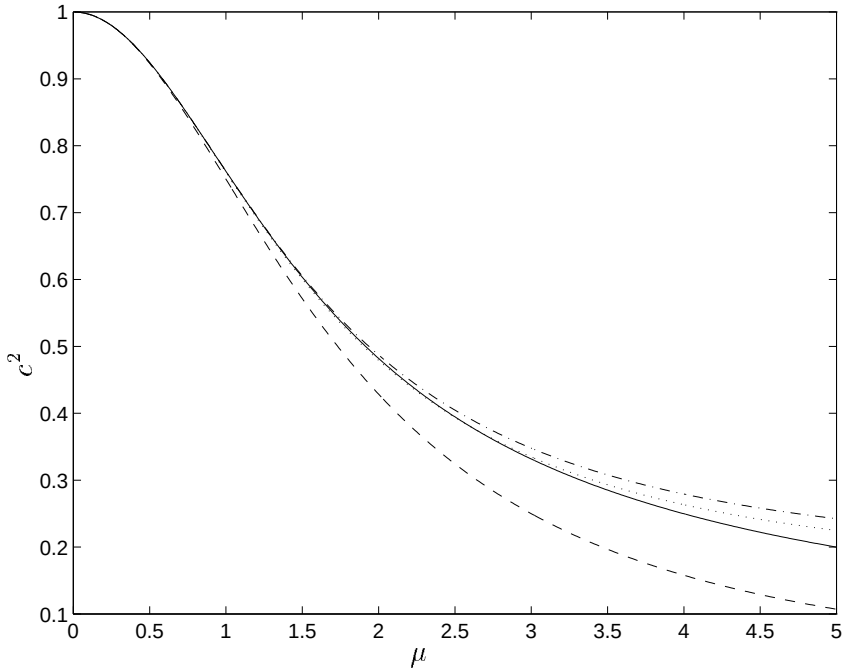

Figure 1: Dependence of linear phase speed c on dimensionless relative depth μ. Solid line, linear theory (64). Dashed line, Boussinesq equations based on depth-averaged velocity (59). Dash-dot line, Boussinesq equations with $\alpha = -2/5$ in (62). Dotted line, Boussinesq equations with $\alpha = -0.39$ in (62).

4 Boussinesq approximations: Hamiltonian formulations

As an alternative to the standard derivation outlined above, several authors have provided derivations of weakly-nonlinear Boussinesq equations based on the Hamiltonian and resulting canonical evolution equations. These results are reviewed here in the simplified context of two-dimensional propagation in water of constant depth h. A detailed review of existing variable depth formulations may be found in Dingemans [45].

Most of the work on Boussinesq approximations through Hamiltonian formulations follows along lines laid out by Broer and associates [46] [47] [48]. The Hamiltonian may be written as the sum of kinetic and potential en-

ergy contributions

$$\mathcal{H} = \mathcal{T} + \mathcal{V}. \tag{66}$$

Introducing the non-dimensionalization of section 2.4 and normalizing $\mathcal{H}$ by $\rho g a^2/2$, we get (in dimensionless form)

$$\mathcal{T} = \int\int_{\mathbf{x}} \int_{-h}^{\delta\eta} \left[\nabla\phi \cdot \nabla\phi + \frac{1}{\mu^2}(\phi_z)^2 \right] dz d\mathbf{x} \tag{67}$$

$$\mathcal{V} = \int\int_{\mathbf{x}} \eta^2 d\mathbf{x}. \tag{68}$$

The difficulty in deriving the canonical evolution equations lies in specifying the canonical momentum $\xi(\mathbf{x}, t)$ in terms of the velocity potential $\phi(\mathbf{x}, z = \eta, t)$. Broer and most subsequent researchers have proceeded by splitting the kinetic energy integral into an integral from the bottom to the mean water level plus an integral from the mean water level to η:

$$\mathcal{T} = \mathcal{T}_0 + \mathcal{T}_\eta, \tag{69}$$

where

$$\mathcal{T}_0 = \int\int_{\mathbf{x}} \int_{-h}^{0} \left[\nabla\phi \cdot \nabla\phi + \frac{1}{\mu^2}(\phi_z)^2 \right] dz d\mathbf{x} \tag{70}$$

$$\begin{aligned} \mathcal{T}_\eta &= \int\int_{\mathbf{x}} \int_{0}^{\delta\eta} \left[\nabla\phi \cdot \nabla\phi + \frac{1}{\mu^2}(\phi_z)^2 \right] dz d\mathbf{x} \\ &= \delta \int\int_{\mathbf{x}} \eta \left[\nabla\phi \cdot \nabla\phi \right]_{z=0} d\mathbf{x} + O(\delta\mu^2, \delta^2) \end{aligned} \tag{71}$$

by virtue of the fact that $\phi_z = O(\mu^2)$ at leading order, and where we introduce a Taylor expansion about $z = 0$ and retain terms appropriate to a weakly-nonlinear formulation. (Note that this approach appears to eliminate the possibility of obtaining a fully-nonlinear formulation, as given in section 3). Subsequent development depends on the assumption that the value of the potential at the surface may be represented in terms of the value at the still water level $z = 0$. Letting $\xi_0(\mathbf{x}, t) = \phi(\mathbf{x}, z = 0, t)$, we may use Green's identity together with Laplace's equation and the bottom boundary condition to replace (70) by

$$\mathcal{T}_0 = \frac{1}{\mu^2} \int\int_{\mathbf{x}} \xi_0 (\phi_z)_{z=0} d\mathbf{x}. \tag{72}$$

It is illustrative to consider the implications of the solution to the full linear problem in the development of the weakly-dispersive approximation here. For waves propagating in constant depth in two dimensions,

the full solution to the problem in an unbounded domain may be written (in dimensional form)

$$\phi(\mathbf{x}, z, t) = \frac{1}{4\pi^2} \int \int_{\mathbf{k}} \hat{\xi}_0(\mathbf{k}) \frac{\cosh k(h+z)}{\cosh kh} \mathrm{e}^{i(\mathbf{k}\cdot\mathbf{x} - \omega(k)t)} d\mathbf{k}, \tag{73}$$

where $k = |\mathbf{k}|$ is the magnitude of the wavenumber vector and $\hat{\xi}_0$ is the Fourier transform of the potential at the still water level. The linearized kinetic energy may then be written as [45] [50]

$$\mathcal{T}_0 = \frac{1}{8\pi^2} \int \int_{\mathbf{k}} |\hat{\xi}_0|^2 k \tanh khd\mathbf{k}. \tag{74}$$

Alternately, using Parseval's theorem, we can write (74) in terms of an integral over space, as

$$\mathcal{T}_0 = \frac{1}{2} \int \int_{\mathbf{x}} \nabla\xi_0 \cdot (h\mathbf{R}_l(\nabla\xi_0))\, d\mathbf{x}, \tag{75}$$

where $\mathbf{R}_l$ is a real, positive-definite operator with a Fourier transform (or symbol) given by

$$\hat{\mathbf{R}}_l = \frac{\tanh kh}{kh}. \tag{76}$$

For the case of weak dispersion ($kh \ll 1$) we can introduce the approximation

$$\frac{\tanh kh}{kh} = 1 - \frac{1}{3}(kh)^2 + O(kh)^4 + ... \tag{77}$$

which corresponds to an operator $\mathbf{R}$ of the form

$$\mathbf{R} = 1 + \frac{1}{3}h^2\nabla^2, \tag{78}$$

which is not a positive-definite approximation to the full integro-differential operator by virtue of the fact that (77) takes on negative values at large kh. The central problem in developing the Boussinesq approximation is then to obtain a replacement for $\mathbf{R}$ of suitable form, so as to maintain positive-definiteness as well as to obtain relatively accurate dispersive properties.

We now return to nondimensional variables and evaluate (70) directly and compare to the results obtained above. Choosing $z_\alpha = 0$ as the reference level in (38), we retain terms to $O(\mu^4)$ in ϕ and obtain the

results (neglecting bottom slope)

$$\begin{aligned}\phi(\mathbf{x},z,t) &= \xi_0 - \mu^2(hz+\frac{z^2}{2})\nabla^2\xi_0 \\ &\quad +\mu^4\left(\frac{5}{24}h^4 - \frac{1}{4}h^2(h+z)^2 + \frac{1}{24}(h+z)^4\right)\nabla^2\nabla^2\xi_0. \quad (79)\end{aligned}$$

Also note that $\xi = \phi(z=\eta) = \xi_0 + O(\delta\mu^2)$, so that ξ_0 may be replaced by ξ in the Hamiltonian for the lowest order Boussinesq model. Using (79) in (72) then gives

$$\mathcal{T}_0 = \int\int_{\mathbf{x}} \nabla\xi\cdot(h\mathbf{R}\nabla\xi)d\mathbf{x}, \quad (80)$$

where

$$\mathbf{R} = 1+\mu^2\frac{h^3}{3}\nabla^2; \qquad \hat{\mathbf{R}} = 1-\frac{1}{3}\mu^2 \quad (81)$$

in agreement with the first two terms in the expansion (77). Combining (68), (71) and (80) gives the expression

$$\mathcal{H} = \int\int_{\mathbf{x}} \nabla\xi\cdot(\delta\eta + h\mathbf{R})\nabla\xi d\mathbf{x}. \quad (82)$$

Use of (21) and (22) then yields the canonical evolution equations

$$\begin{aligned}\eta_t &= -\nabla\cdot[H\nabla\xi] - \mu^2\frac{h^3}{3}\nabla^2\nabla^2\xi, \quad (83)\\ \xi_t &= \frac{\delta}{2}\nabla\xi\cdot\nabla\xi - \eta, \quad (84)\end{aligned}$$

The problems imposed by the non-positive definiteness of the operator (81) and resulting Hamiltonian (82) may be seen by examining the dispersion relation for the linearized version of (83)-(84), given by

$$c^2 = 1-\frac{1}{3}\mu^2. \quad (85)$$

Note that c takes on imaginary values for values of $\mu = kh > \sqrt{3}$, indicating the instability of short wave solutions to the problem. This is a large value of μ by the standards originally applied to Boussinesq-type models but falls well within the range of accurate prediction capability of models with extended accuracy. In addition, since short waves on the scale of $2\Delta x$ are certain to arise in numerical calculations, the present model may not be used as the basis for numerical calculations

unless heavy short-wave damping is artificially imposed. This damping, in turn, makes the replication of steep nonlinear wave features impossible in a practical sense.

It is thus necessary to alter (82) in such a way that short wave instabilities are avoided. From an *ad-hoc* point of view, this end may be achieved simply by replacing the operator $\mathbf{R}$ by another having a more suitable symbol, and hence a well behaved linear dispersion relation; for example, the choice

$$\hat{\mathbf{R}}_1 = \frac{1-(\alpha+1/3)\mu^2}{1-\alpha\mu^2}; \qquad \mathbf{R}_1 = \frac{1+(\alpha+1/3)h^3\nabla^2}{1+\alpha h^3\nabla^2} \tag{86}$$

reproduces the extended dispersion relation of Nwogu's model (62) and gives the modified evolution equations

$$(1+\mu^2\alpha\nabla^2)\eta_t = -\nabla\cdot[H\nabla\xi] - \mu^2(\alpha+\frac{1}{3})h^3\nabla^2\nabla^2\xi + O(\delta\mu^2,\mu^4) \tag{87}$$

together with (84). Most authors take the additional step of replacing (82) with a quadratic form, thus guaranteeing positive-definiteness. For example, Mooiman [50] introduces the quadratic form

$$\mathcal{H} = \int\int_{\mathbf{x}} \left[H(\mathbf{G}\nabla\xi)^2 + \eta^2\right] d\mathbf{x}, \tag{88}$$

which corresponds to the canonical evolution equations

$$\eta_t = -\nabla\cdot(\mathbf{G}^*(H\mathbf{G}(\nabla\xi)) \tag{89}$$

$$\xi_t = -\frac{\delta}{2}\left(\mathbf{G}(\nabla\xi)\right)^2 - \eta, \tag{90}$$

where $\mathbf{G}^*$ is defined such that $\widehat{\mathbf{G}^*\mathbf{G}} = \hat{\mathbf{R}}_l$ to the required order of approximation. Mooiman makes the choice

$$\mathbf{G} = \mathbf{G}_{a,b} = \mathbf{L}_b^{-1}\mathbf{L}_a; \qquad \mathbf{L}_\gamma = 1 - \mu^2\frac{\gamma}{6}h^2\nabla^2. \tag{91}$$

Requiring $\mathbf{G}$ to reproduce the leading order Taylor series behaviour of $\mathbf{R_l}$ in (81) leads to the condition

$$b - a = 1 \tag{92}$$

and a resulting linear dispersion relation

$$c^2 = \hat{\mathbf{G}}^2 = \left(\frac{1+\frac{a}{6}\mu^2}{1+\frac{b}{6}\mu^2}\right)^2. \tag{93}$$

Based on comparisons with the exact dispersion relation, Mooiman suggested the choice of parameters $b = 1.9, a = 0.9$. However, as shown in Figure 2, it is not clear that this is the best choice over a range of values of $\mu = kh$ appropriate to the intermediate depth problem.

Values closer to $b = 1.7, a = 0.7$ would seem to provide a better fit. It is also clear that models that reproduce the Padé form of the dispersion relation provide a more accurate representation of the dispersion relation over this same range.

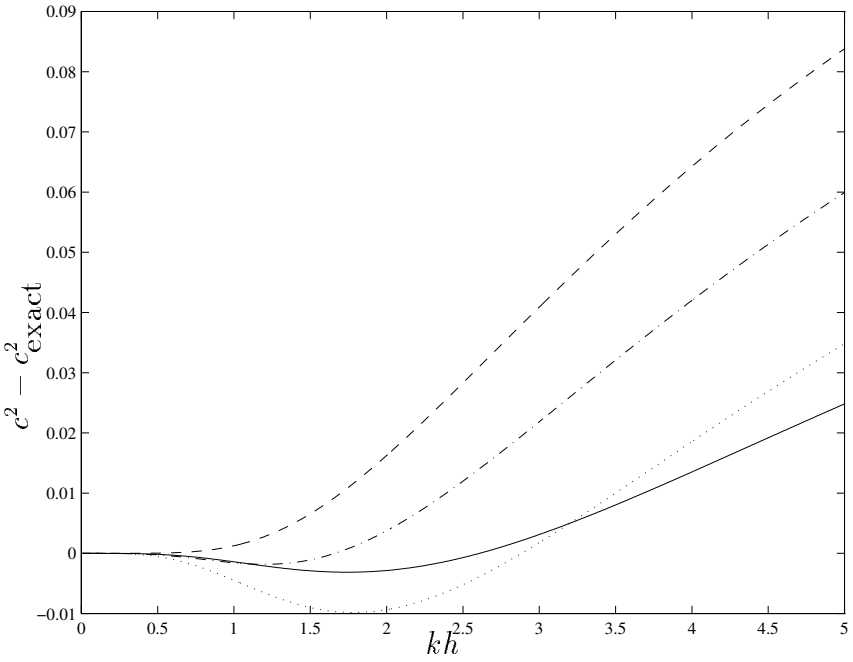

Figure 2: Squared linear phase speed for model equations relative to squared phase speed for exact relation (64). Solid line, Padé approximant (62) with $\alpha = -2/5$. Dashed line, Mooiman model (93) with $b = 1.9$. Dash-dot line, Mooiman model (93) with $b = 1.8$. Dotted line, Mooiman model (93) with $b = 1.7$.

Additional derivations of weakly-nonlinear Boussinesq models have been provided by Van der Veen & Wubs [51] and Yoon & Liu [52]. In particular, the model of Van der Veen & Wubs reproduces the Padé form of the linear dispersion relation and may thus be expected to predict re-

sults with comparable accuracy to those of the Nwogu or other extended weakly-nonlinear model equations.

5 Serre equations

An independent line of approach to the derivation of evolution equations has been pursued by several authors starting with Serre [33]. In this approach, a model for the internal flow field is adopted in which the horizontal velocity is assumed to be uniform over depth and the vertical velocity varies linearly from the bottom to the free surface. Models are then developed by obtaining appropriate integrals over depth of the Euler equations and applying surface boundary conditions. The dependent velocity variable is thus the depth-averaged velocity $\overline{\mathbf{u}}$, which coincides with the local horizontal velocity over the entire water column. To date, applications of the resulting approach have been limited to one horizontal dimension (taken to be x). Extensive details on model derivations may be found in Dingemans [45].

Note that the assumed form of the kinematics in these models implies that the computed flow field is rotational. For motion in the x, z plane, we have vorticity $\omega = \partial w/\partial x = O(\mu^2)$, and thus vorticity enters the flow field description at the same order as the leading order dispersive terms.

Serre-type models are derived assuming a particular relation between scaling parameters δ and μ. For the case where the usual weakly-nonlinear Boussinesq approximation is employed ($\delta = O(\mu^2)$), Dingemans [45] shows that the derivation reproduces the equations of Peregrine [9] written in terms of depth-averaged velocity. Serre [33] and Su & Gardner [34] employed the relation $\delta = O(\mu)$, which leads to the retention of some nonlinear effects in dispersive terms in the resulting model equations. For the case of a horizontal bottom, Serre and Su & Gardner obtained the set of equations [54]

$$\eta_t + (Hu)_x = 0 \tag{94}$$

$$u_t + \delta u u_x + \eta_x + \frac{2}{3}\mu^2 H_x \Gamma + \frac{1}{3}\mu^2 H \Gamma_x = 0, \tag{95}$$

where u is the x-component of $\overline{\mathbf{u}}$ and

$$\Gamma = H(\delta(u_x^2 - u u_{xx}) - u_{xt}). \tag{96}$$

These equations are fully equivalent to the model equations (44) and (45), which are derived with the assumption that the horizontal velocity profile has a quadratic variation over the depth. It is apparent that this variation does not influence the resulting governing equation when depth-averaged velocity is chosen as the dependent variable.

Equations (94)-(96) have an exact solitary wave solution, given by

$$\eta = \cosh^{-2}\left[\frac{K}{h}(x-ct)\right] \tag{97}$$

$$u = \frac{c\eta}{H}, \tag{98}$$

with $K = (3\delta/4(1+\delta))^{1/2}$ and $c = 1/(1+\delta)^{1/2}$ and where the nonlinear parameter δ describes the ratio of wave height over water depth. In comparison, K for the solitary wave solution of the KdV equation (132) is given by $K = 3\delta/4$. The Serre solution produces solitary wave crests which are quite broad relative to either exact solutions or to solutions based on the weakly or fully-nonlinear Boussinesq models of the previous section. In Figure 3, we show a comparison of solitary waves based on the accurate numerical solution of Tanaka [53] (solid lines), the weakly nonlinear KdV solution (dashed line), a numerical solution of the fully nonlinear Boussinesq equations (52) - (53) [55] (dash-dot line), and the present solution of the Serre equation (dotted line). The figure shows that the fully-nonlinear Boussinesq model provides a highly accurate reproduction of the exact solitary wave shape up to very high wave heights. In contrast, the wave crest predicted by Serre equations is quite broad and becomes broader as height increases, relative to any other solution technique.

Seabra-Santos *et al* [54] have provided a variable-depth form of the Serre equations given by

$$\eta_t + (Hu)_x = 0 \tag{99}$$

$$H(u_t + \delta u u_x) + \left[H^2(\frac{1}{2}(1+\Sigma) + \frac{1}{3}\Gamma)\right]_x = Hh_x(1+\Sigma+\frac{1}{2}\Gamma) \tag{100}$$

with

$$\Sigma = -h_x(u_t + \delta u u_x) - \delta h_{xx} u^2. \tag{101}$$

Finally, we note that the linearized dispersion relation corresponding to the models described here is the relation (59), which requires

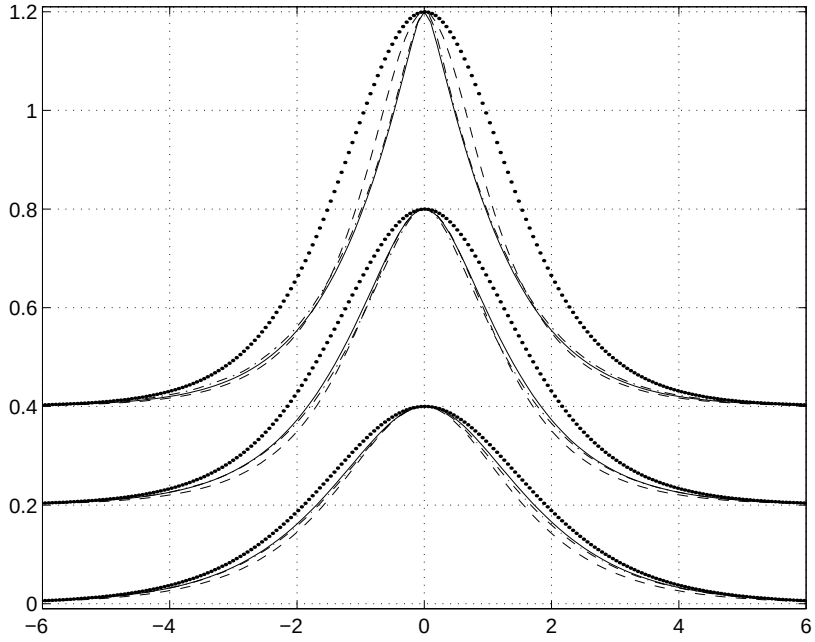

Figure 3: Comparison of solitary wave shapes for wave heights $\delta = 0.4, 0.6, 0.8$. Solid line - Tanaka's solution. Dashed line - KdV solitary wave solution. Dash-dot line - numerical solution of fully nonlinear Boussinesq equations (52) - (53). Dotted line - Serre equation solution (97) - (98)

improvement before the models can be used to model waves in intermediate depths. Steps in this direction, leading to a corrected equation which retains depth-average velocity, have been made [66] but are largely undocumented to date. However, it is apparent that the fully-nonlinear Boussinesq model (52)-(53) provides such a correction and does an excellent job of predicting the form of solitary wave crests.

6 Green-Naghdi (GN) equations

The final method for obtaining approximate governing equations considered here is the method of Green & Naghdi [56] [35]. In this approach, an assumption is made about the kinematic properties of the velocity field,

after which conservation laws governing the coefficients of the velocity field are derived. The original approach to the problem [56] used the theory of directed fluid sheets or Cosserat surfaces. Green & Naghdi [35] provide a parallel derivation of their approximate equations based on the explicit conservation laws for inviscid fluid flow. These equations are now commonly referred to as Green-Naghdi or GN equations. In this formulation, the method takes on something of the flavour of a Galerkin approximation of the full problem, using the assumed form of the velocity field as the shape function. The resulting models are fully nonlinear, as no scaling assumptions are made about the relative height to depth ratio and all boundary data are evaluated at the instantaneous free surface.

The original GN model uses the same kinematic assumption as the Serre model; a linear variation of vertical velocity over depth and a depth-uniform horizontal velocity. The equations of Green & Naghdi can be written in the present notation following Miles & Salmon [57]; see also [58]

$$\eta_t + \nabla \cdot (H\overline{\mathbf{u}}) = 0 \tag{102}$$

$$\overline{\mathbf{u}}_t + \delta\overline{\mathbf{u}} \cdot \nabla\overline{\mathbf{u}} + \nabla\eta = -\mu^2\mathbf{A}, \tag{103}$$

where

$$\mathbf{A} = \frac{1}{3H}\nabla(H^2D^2\eta) \tag{104}$$

for uniform depth and

$$\mathbf{A} = \frac{1}{6}\left\{\nabla\left[HD^2(2\eta - h)\right] + (\nabla\eta)D^2(2\eta - h) + (\nabla h)D^2(2h - \eta)\right\} \tag{105}$$

for variable depth, where $D() = ()_t + \overline{\mathbf{u}} \cdot \nabla()$ and where we retain the notation $\overline{\mathbf{u}}$ for the uniform-over-depth horizontal velocity. As is the case with the Serre equations, (102)-(103) represents a system having non-zero vorticity. Miles & Salmon [57] consider the vorticity and show that a potential vorticity may be derived and is conserved by the system for any motion starting from rest. Calculations for upstream-advancing solitons generated by ships moving at transcritical speed have been made by Ertekin *et al* [58]. There has been very little direct comparison to data for this particular model system.

Owing to the similarity in the assumed velocity profiles, one would suspect that the Serre and GN models should bear a striking resemblance. To investigate this, we may rewrite (102) as

$$D\eta = -Hu_x \tag{106}$$

for the case of constant depth and propagation in one dimension. The expression for $D^2\eta$ then becomes (in 1-D)

$$D^2\eta = H[\delta(u_x^2 - uu_{xx}) - u_{xt}] = \Gamma \tag{107}$$

where Γ is defined in (96). Expanding the one-dimensional version of (103) then gives (95) identically, proving the equivalence of the models. Based on this correspondence, we may write a two-dimensional version of Γ as

$$\Gamma = H\left\{\delta[(\nabla\cdot\overline{\mathbf{u}})^2 - \overline{\mathbf{u}}\cdot\nabla(\nabla\cdot\overline{\mathbf{u}})] - \nabla\cdot\overline{\mathbf{u}}_t\right\} \tag{108}$$

thus extending the Serre equations to two horizontal dimensions.

As is the case with the other weakly dispersive models described here, the leading order GN model needs to be extended to include more accurate linear dispersion effects before it can be applied to intermediate depth propagation. Shields & Webster [59] [60] have provided a framework for such an extension. They proceed by writing the velocity field (in the present notation) as

$$\boldsymbol{u}(\mathbf{x},z,t) = \sum_{n=0}^{K}\mathbf{W}_n(\mathbf{x},t)s^n, \tag{109}$$

where K is a finite integer corresponding to the level of the resulting model, and where s is the vertical position in a mapped coordinate system which places the bottom at $s=-1$ and the water surface at $s=1$. Equations are then found which govern the evolution of the $\mathbf{W}_n$, and which satisfy mass conservation and the kinematic surface boundary condition. The Euler equations are satisfied in an approximate sense, using a weak variational formulation in which the basis functions of (109) are used as weighting functions. The resulting system consists of K equations for the amplitudes of the velocity field together with an equation governing the change in thickness of the water column. Further details may also be found in Demirbilek & Webster [61]. To date, these theories have only been implemented for one horizontal direction.

Shields & Webster [59] have shown calculations of solitary waves and regular cnoidal waves for GN models up to level three, and have shown that convergence towards numerically exact results for wave shape and wave speed is more rapid than for corresponding perturbation series. Calculations of waves shoaling in variable depth are also provided by Shields [62], who shows good agreement between wave height evolution

and wave shape for shoaling periodic waves, in comparison to laboratory data [63]. Additional example calculations are provided by Demirbilek & Webster [64]. Webster & Wehausen [65] have also applied the method to the problem of resonant Bragg reflection of surface waves by undular bed features.

7 Model performance

The testing of existing modelling schemes has been fragmentary, especially with regard to model intercomparisons relative to single data sets or more exact calculations. The principal exception to this is provided by Dingemans [66], who has provided a comparison of calculations of nine models to a single laboratory data set. The main issues to be addressed in testing of the models include accuracy of intermediate depth linear propagation (including dispersion, shoaling, refraction and diffraction), and reproduction of nonlinear wave features during the final stages of shoaling and wave breaking. In addition, the question of whether extended Boussinesq models give accurate predictions of nonlinear features in intermediate water depths is of some importance, and has not been adequately addressed to date. An outline of available results and significant findings is provided here.

7.1 Intermediate depth propagation

Several experiments have been performed which provide accurate data sets for intermediate depth waves propagating over bathymetry. The data set of Berkhoff *et al* [67], for wave focusing over a submerged shoal, has been extensively used to test the performance of parabolic model schemes [68]. A schematic of the bottom geometry is shown in Figure 4. Kirby and Dalrymple [69] showed that the experimental results are significantly affected by nonlinearity, and that parabolic model schemes that account for the leading order, self-interaction effect in Stokes wave theory are capable of reproducing the focusing behaviour (including the effect of nonlinear defocussing) observed in the experiment. In addition, waves in the experiment propagate from a relatively deep region, where $kh \sim 2$, to much shallower depths. This experiment is thus ideal for testing the intermediate depth shoaling and nonlinear properties of the

extended Boussinesq schemes developed above. Wei and Kirby [70] performed such a comparison using the weakly-nonlinear Nwogu equations. Their published results were inaccurate, due to problems with the incident wave boundary condition as well as a misinterpretation of whether the model had reached an asymptotic steady periodicity. Corrected results for a comparison of measured and computed wave heights for the measurement transects shown in Figure 4 are shown in Figure 5. The results show close agreement with data, with prediction accuracy similar to that available using large-angle parabolic model schemes [68]. These results are not changed in any significant way when the fully nonlinear formulation is used. Similar results using a model based on Hamilton's principal have been shown by Mooiman [71].

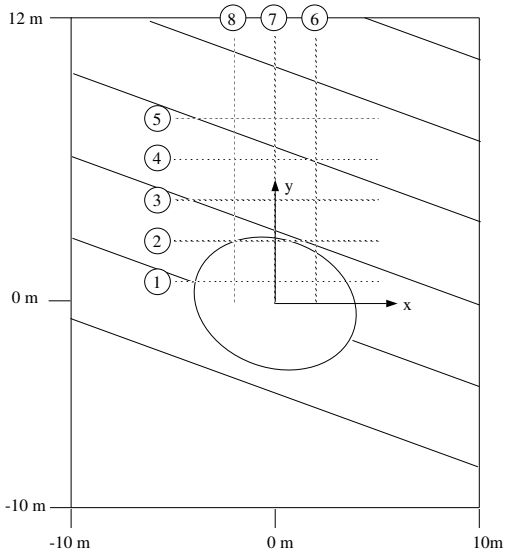

Figure 4: Geometry of submerged shoal experiment of Berkhoff *et al* [67] including measurement transects (from [70]).

7.2 Solitary waves on a plane beach

Waves close to the break point can often have height to depth ratios larger than one during their rapid unsteady evolution, and thus the restrictions of a weakly nonlinear theory are dramatically violated during the final

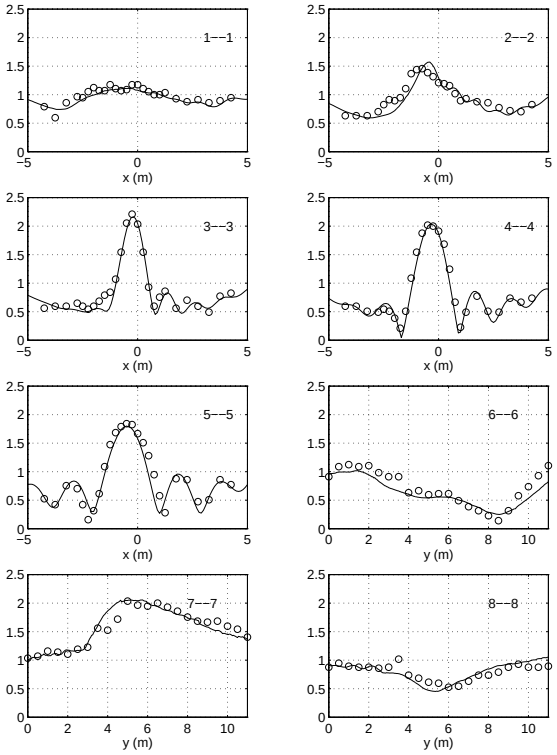

Figure 5: Comparison of measured (circles) and computed crest-to-trough wave heights for submerged shoal experiment [67][70].

stages of shoaling. The problem of wave evolution close to breaking thus provides an excellent test of the relative accuracy of weakly-nonlinear and fully-nonlinear versions of the Boussinesq models. Wei *et al* [43] have studied the shoaling of solitary waves up to the break point, and have compared results from the weakly-nonlinear model (55) - (56) and the fully-nonlinear model (52) - (53) to results obtained using an accurate boundary integral solution [24]. The solitary wave test is a good choice for performing model comparisons, since the wave can be started inside the model domain and there are no initial transients or other features in the solution resulting from boundary treatments, which can cloud an evaluation of the basic models.

Wei *et al* considered solitary waves of three initial heights, each shoaling over 4 different beach slopes. Results showed that weakly-nonlinear

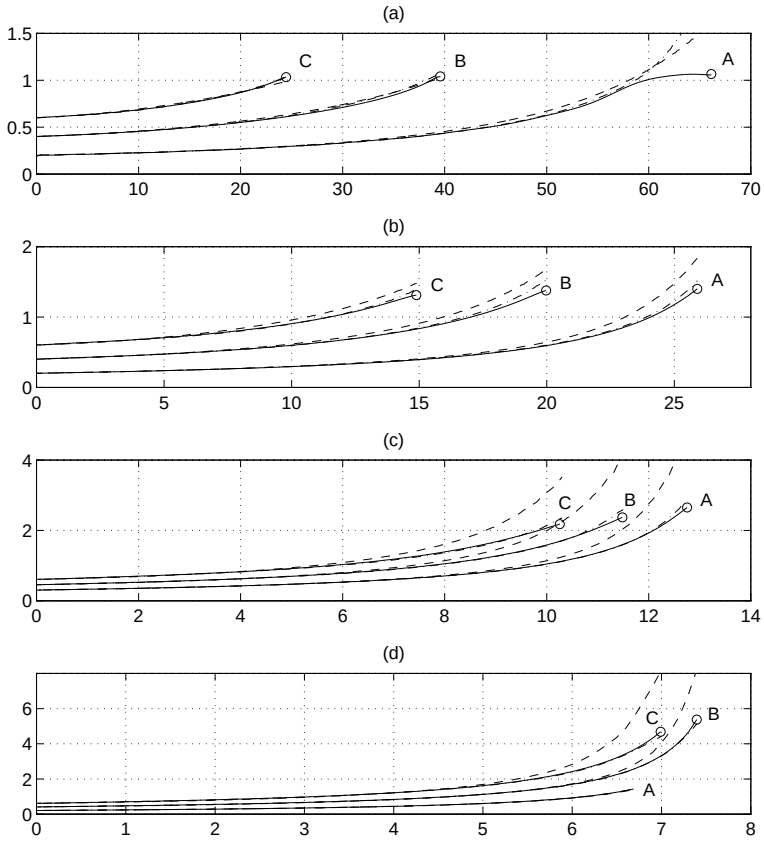

Figure 6: Comparison between boundary integral model (solid lines), weakly nonlinear Boussinesq model (dashed lines) and fully nonlinear Boussinesq model (dash-dot lines) of shoaling rates H/h for solitary waves with δ = (A) 0.20, (B) 0.40, (C) 0.60 in (a),(b),(d) and δ = (A) 0.30, (B) 0.45, (C) 0.60 in (c); shoaling on a slope: (a) 1:100; (b) 1:35; (c) 1:15; (d) 1:8. Circle symbols denote locations of the breaking point for which the wave has a vertical tangent on the front face in the boundary integral computations. (From [43]).

Boussinesq calculation consistantly showed an overprediction of wave height as waves approached the break point, together with overly narrow and curved crests (and resulting high horizontal velocities.) In contrast, the fully-nonlinear model equations provided an accurate prediction of wave height evolution (see Figure 6) as well as accurate reproduction of wave shape and magnitude of maximum horizontal velocities. The predicted point where horizontal velocity at the wave crest coincides with the crest translational speed, which would be an indication of limiting wave height from a physical point of view, agreed closely with the predicted point of the onset of breaking in the boundary integral calculations. Overall, the significance of the additional nonlinear effects in the final stages of shoaling was quite clear.

7.3 Additional model intercomparisons

Dingemans [66] has provided a comparison between the predictions of seven weakly dispersive wave models, a boundary integral model, a fully-dispersive model based on canonical Hamiltonian evolution equations, and a laboratory data set. The lab experiment considered the shoaling of an initially sinusoidal regular wave over a bar with sloping sides. The bar height occupied 75% of the water depth at the crest. Waves shoaled significantly over the bar and broke over the bar crest in one of the three cases studied. The strongly deformed waves then propagated back into relatively deep water on the lee side of the bar, and the waves decomposed into a fundamental and free higher harmonics with only weak nonlinear interactions. The experimental data thus provides a strong test of the linear dispersive characteristics of the models as well as their ability to reproduce strong nonlinear distortions during the shoaling process. Tests with breaking were not a primary focus of the comparison study. For a case with moderately long initial waves ($2s$ period in $0.8m$ of water), the study showed fairly conclusively that the primary consideration affecting model performance was the accuracy of the model dispersive properties, with the retention of higher order nonlinear effects being a distinguishing feature only after correction of the dispersive properties. In this instance, the best model performance in the group of long wave models was found in an undocumented Serre model with corrected dispersive properties due to Barthélemy & Guiborg of LEGI-IMG (see [66] for details of model formulation). This conclusion unfortunately did not survive to the next case studied, which used a shorter but steeper incident wave. In this

instance, the weakly-nonlinear Boussinesq models of Madsen *et al* [39] and Mooiman [50] outperformed the Serre model with corrected linear dispersion. This result was unexpected but may be another indication of the Serre-type model tending to deviate from accurate solutions as steepness increases, as indicated in the solitary wave comparison above.

8 Additional physical effects

The models described to this point represent the propagation of waves seaward of the surf zone, in the range where friction is negligible and energy is essentially conserved. A comprehensive model of near-shore processes needs to be able to describe the additional complexity of surf zone wave behaviour, including wave breaking and runup on the shoreface. The breaking process is not described by the basic framework given above. In addition, the process of fluid motion in the swash zone occurs in a regime where the dispersive properties of the Boussinesq model are not appropriate. Nevertheless, there has been a great deal of progress made in extending the range of weakly dispersive models into the surf zone, and thus providing a comprehensive model of wave motion in the coastal environment.

8.1 Wave breaking

The application of the Boussinesq models in the surf zone region is problematic from the viewpoint of consistency. Nonlinearity becomes strong ($\delta \to O(1)$) while dispersive effects should disappear ($\mu^2 \to 0$). In this limit, the Boussinesq model would approach the usual NSW equations. These equations predict the eventual steepening and 'breaking' (manifested through the convergence of solution characteristics) of any initial wave form, and thus do not allow for the modelling of non-breaking waves over any appreciable distance. The NSW equations provide a successful and well tested framework for modelling the dissipation and runup of surf zone waves [72] [73] [74] [75]. The numerical approach is usually based on the Lax-Wendroff scheme or similar dissipative schemes which preserve the mass and momentum conserving properties of the governing equations, but which dissipate energy. This approach provides predictions of surf zone wave heights, fluid velocities and skewness and asymmetry statistics which are in reasonable agreement with measurements [76]. The

approach has the disadvantage that the modeller does not have control over the dissipative processes involved, which, in turn, are not specified by any physically based model. Finally, the NSW equations cannot accurately predict the propagation of incident waves seaward of the surf zone.

In contrast, the schemes utilized to solve the Boussinesq equations typically are at least intended to be conservative of mass, momentum and energy, and do not form weak solutions or shocks as the wave fronts steepen. Instead, the increased wave front curvature leads to an increase in the effect of dispersive terms as water depth decreases, rather than a decrease. Since the schemes are basically conservative, the equations respond to the increased curvature by radiating shorter waves which are slower and hence trail behind the main wave crest. This effect is equivalent to the undular bore phenomenon seen in low Froude number hydraulic jumps [77], the difference being that breaking would not occur and replace the tendency to radiate the short waves as wave height increased beyond some value. It is up to the modeller to invoke a dissipation mechanism and include it in the model equations.

A number of different models for wave breaking effects have been used to date. These models can be roughly separated into two groups: models where the rate of dissipation depends on some geometric or global (in time or space) property of the wave train, and models where the rate of dissipation is determined entirely by local (in time or space) properties. Within each group, it is further possible to distinguish two basic techniques for achieving a damping effect: use of an eddy viscosity formulation, or use of an applied pressure distribution.

Eddy viscosity models have the longest history in application. These involve extending the momentum equation by the addition of a dissipation term, indicated schematically by

$$u_t + \delta u u_x + \eta_x - (\nu_b u_x)_x + \text{dispersive terms} = 0 \qquad (110)$$

Note that some authors [78] [79] write the additional term with the eddy viscosity coefficient outside the second derivative. This implies that a contribution to flow momentum is imposed when breaking occurs, in contrast to the momentum-conserving bore process in the non-dispersive theory. In situations where dissipation is imposed globally and spatial variations in ν_b over a wave period are small, this effect is minor. However, at the onset of breaking or in models where dissipation is localized

and spatial gradients of viscosity are large, this momentum source effect can be quite severe, and should be avoided by correctly specifying the dissipation term.

Karambas *et al* [78] provide an example formulation where ν_b is calculated, based on a mixing length hypothesis and then applied globally over the waveform. No comparisons to data are provided.

Zelt [80] has utilized a spatially localized eddy viscosity formulation [81] based on a mixing length hypothesis. Following Zelt, ν_b is given by

$$\nu_b = -l^2 u_x, \tag{111}$$

with the mixing length l given by

$$l = B\gamma H. \tag{112}$$

Heitner and Housner [81] chose $\gamma = 2$ based on comparisons between numerical results and experiments on the width of the bore region in a steady hydraulic jump. The factor B is used to introduce a breaking criterion and is given by

$$B = \begin{cases} 1; & u_x \leq 2u_x^* \\ u_x/u_x^* - 1; & 2u_x^* < u_x \leq u_x^*, \\ 0; & u_x > u_x^* \end{cases} \tag{113}$$

where u_x^* is a critical velocity gradient taken to be

$$u_x^* = -0.3\sqrt{\frac{g}{h}}. \tag{114}$$

In practice, the expression (112) is linearized to give $l = B\gamma h$, and a smoothing filter is used to smooth the computed ν_b distribution slightly. Zelt [80] used this formulation in the context of a weakly-nonlinear Boussinesq model in Lagrangian coordinates and studied the breaking and runup of solitary waves on a plane slope, and obtained reasonable agreement with laboratory data [82]. More recently, Wei and Kirby [55] have used this method to study the breaking of a random wave train over a plane slope. Wei and Kirby used the laboratory data of Mase and Kirby [83], who considered the propagation of a wave train corresponding to a Pierson-Moskowitz spectrum over a 1:20 beach slope. An example of 30 seconds of run time is shown in Figure 7, where the initial measurement at a depth of 47 cm is shown together with shoaled, breaking

waves at $h = 17.5, 15, 12.5, 10, 7.5, 5$ and 2.5 cm progressing up the figure. These tests were conducted with a peak frequency of about 1 Hz, corresponding to a value of $kh \sim 2$ in the deeper part of the tank. The Nwogu-type model with improved dispersion was used as the basis for calculations. Computations using the model based on depth-averaged velocity (44) and (46) were also attempted and failed to reproduce the shoaling and propagation of the shorter wave components in the wave train, as would be expected for waves starting in this large a depth. The calculations shown here reproduce the arrival time of individual waves as well as the height and general shape of waves in the surf zone.

Statistical measures based on the entire experimental series (covering about 800 waves) were computed. Figure 8 shows computed and measured third-moment statistics for an entire run, and indicates that the simple eddy viscosity formulation is capable of providing accurate predictions of wave skewness and asymmetry, which are important for the subsequent calculation of sediment transport properties.

Karambas & Koutitas [79] have provided a much more elaborate scheme for computing the eddy viscosity ν_b using an energetic eddy length scaling rather than a mixing length based on the total depth. They obtain good prediction of decaying wave heights in the surf zone, as compared to regular wave data from several sources. They also provide setup calculations which show a large underprediction relative to measured data. This underprediction may well be due to the incorrect positioning of the eddy viscosity in the model dissipation term in their formulation, which would lead to a modification of the cross-shore time-averaged momentum balance.

An alternate formulation based on a *surface roller* concept [84] [85] has been described by Schäffer *et al* [86]. Using a weakly-nonlinear Boussinesq formulation based on surface displacement and depth-integrated volume flux, they formulate the model (written in the present notation)

$$\eta_t + P_x = 0 \quad (115)$$

$$P_t + \left(\frac{P^2}{H}\right)_x + R_x + \eta_x + \mu^2 \left[\frac{h^3}{6}\left(\frac{P}{H}\right)_{xxt} - \frac{h^2}{2}P_{xxt}\right] = 0, \quad (116)$$

where $P = Hu$ and where R is a pressure-like imposed force specified by the roller model. R is found to be an excess momentum effect which can be written as

$$R = M - \frac{P^2}{H}, \quad (117)$$

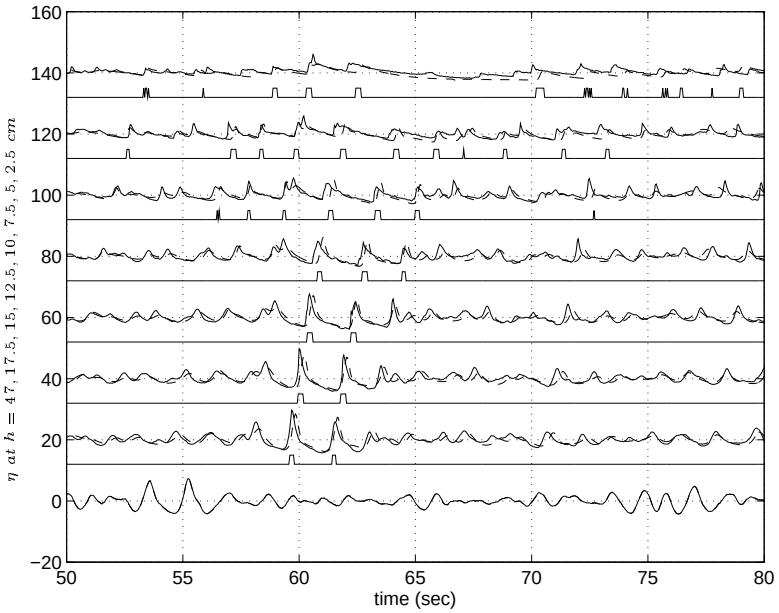

Figure 7: Comparison of surface elevation at different water depths. Solid line - experimental data [83]. Dashed line - numerical calculation based on (52) - (53). Isolated blips on records under wave records indicate temporally localized breaking. (From [55]).

where M is the actual momentum flux computed using the true vertical distribution of horizontal velocity, including breaking and turbulence effects. The main assumption in the model development thus revolves around the choice of the assumed velocity profile. Schäffer *et al* choose a simple two-layer model where the roller region is taken to be a simple quiescent mass of water translating at the phase speed of the underlying wave. Note that in this formulation, where R takes on non-zero values only near the front of breaking wave crests, the overall average momentum balance is not affected by the additional term.

Numerical calculations with this model also provide good predictions of wave height decay, and additionally provide accurate prediction of surf zone setup. Additional results using this formulation may be found in Madsen *et al* [87]. The same general approach has also been used by Brocchini *et al* [88] in both a Boussinesq and Serre model.

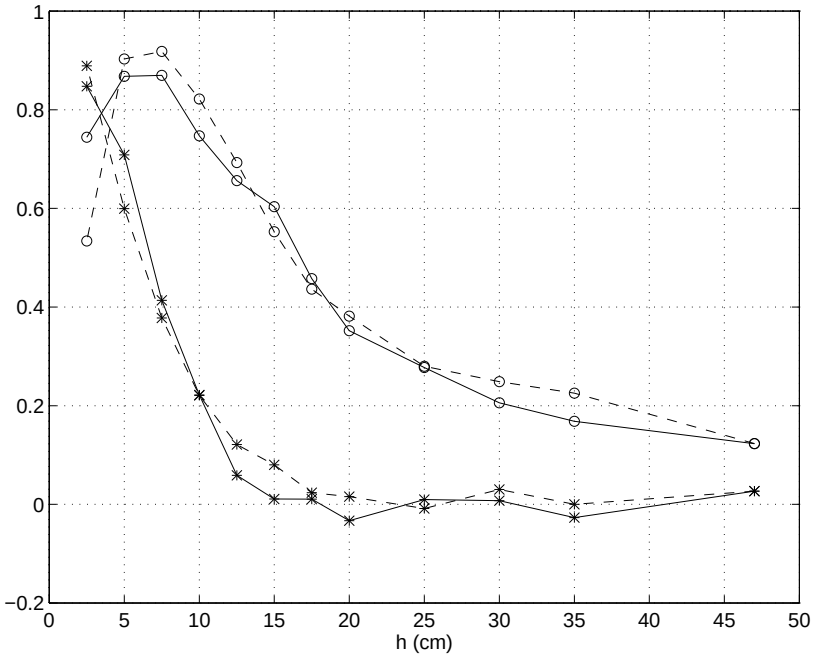

Figure 8: Comparison of skewness (circles) and -asymmetry (stars) at different water depths. Solid lines - experimental data [83]. Dashed lines - numerical computations based on (52) - (53). (From [55]).

8.2 Runup

Modelling the complete wave transformation process in the cross-shore direction requires a treatment of the movement of the water line on the inclined shore face. The problem of modelling runup on the shore face does not introduce major new physical considerations in the modelling scheme (unless percolation effects are to be considered). Instead, the problems presented are primarily numerical and are associated with the movement of the boundary of the fluid domain in a fixed horizontal coordinate system. There are several approaches to the solution of this problem which are described in the literature, which can be categorized roughly as:

1. coordinate transformation techniques, in which a mapped coordinate follows the water edge;

2. grid draining and filling techniques;

3. techniques which treat the entire modelled domain as part of the active fluid domain.

The first category of models is exemplified by models developed in Lagrangian coordinates. For the particular case of purely cross-shore motion, use of Lagrangian coordinates renders the shoreline stationary, and thus the runup problem is essentially solved. Pedersen and Gjevik [89] reported calculations of the runup of solitary waves using a Boussinesq model written in Lagrangian coordinates, and obtained good agreement with laboratory data. This approach was extended by Zelt [80], who incorporated the breaking model described above and studied the runup of both breaking and non-breaking solitary waves, again obtaining good results. This approach can, in principal, be extended to two-dimensional problems having longshore as well as cross-shore shoreline movement. Use of a purely Lagrangian scheme for surf zone applications is problematic, however, since the mean flow developed by breaking waves would tend to advect the grid longshore relative to the stationary region of interest. It is possible to adopt semi-Lagrangian schemes, where only the cross-shore motion is treated in a Lagrangian framework. Alternatively, simple coordinate stretching techniques may be utilized which strain the model grid in the cross-shore direction in order to follow the moving shoreline. This approach has been used by Özkan & Kirby [90] in schemes for longshore runup using the NSW equations.

The second category of shoreline treatments has a long history in the context of storm surge and tsunami runup calculations. In this approach, the water level in the most shoreward active grid in the numerical fluid domain is checked. The shoreline is moved landward if the water level exceeds a critical value or the grid is drained and inactivated if the water level falls below a second critical value. This technique is most applicable in explicit numerical schemes which are not impacted by the change of a grid dimension. Liu et al [92] provide a recent example of this approach, again in the context of long wave runup in the NSW equations.

Finally, there have been several approaches aimed at maintaining an active computational grid over an entire pre-specified model domain containing subaerial regions. Madsen *et al* [87] describe the application of a method due to Tao [93] in which the solid seabed is replaced by a network of very narrow vertical slots superimposed on the original

topography. Water is assumed to occupy all of the network of slots up to the original still water level, and thus the entire model grid is active from the start. As the shoreline advances, slots fill until the water level reaches the original bed level, after which water flows over the newly submerged bed. In a sense, the method is analogous to coupling the fluid domain to a porous bed, in which the level of porosity is then made as small as possible. Madsen *et al* show a comparison for regular wave runup to the analytic solution of Carrier & Greenspan [91] and show that the level of apparent porosity in the numerical scheme must be very carefully controlled in order to obtain accurate runup calculations. They also found that it was neccessary to turn off the dispersive terms in the model as the runup tip is approached.

An alternate approach to the problem of maintaining an active fluid domain everywhere uses the approach of imposing a bottom friction term, which becomes extremely large as the local total depth approaches zero, thereby 'freezing' a thin layer of fluid on an otherwise subaerial region [94].

Following this approach, Wei & Kirby [55] added a bottom friction term of the form

$$\mathbf{F}_b = -\frac{\mathbf{u}_\alpha|\mathbf{u}_\alpha|}{C_f^2 H} \tag{118}$$

and maintained an active grid over the entire domain by imposing a minimum total depth. This method also requires a suppression of the model dispersive terms at the runup tip, since the large curvature of the water surface as the fluid jumps from near-zero to finite depth tends to generate large short-wave oscillations on the scale of the grid spacing.

8.3 Waves on currents and mean current generation

Although the Boussinesq model is most often thought of as a wave propagation model, it contains the framework for the computation of steady or low-frequency motions driven either by imposed currents at boundaries or by the time-average of products of short wave components. This may be seen directly by splitting the velocities and surface displacement into wavy and slowly varying components, and then averaging the resulting equations to obtain separate equations for waves and currents. As an illustration of the results, consider the decomposition of the surface

displacement η and velocity field $\overline{\mathbf{u}}$ into a current-induced part and a wave-induced part

$$\begin{aligned} \eta &= \eta_c + \eta_w \\ \overline{u}_i &= u_{ci} + u_{wi}, \end{aligned} \tag{119}$$

where we will use tensor notation for convenience. Peregrine's [9] equations may be written as

$$\eta_t + [H\overline{u}_i]_{,j} = 0 \tag{120}$$

$$\overline{u}_{i,t} + \delta\overline{u}_j\overline{u}_{i,j} + \eta_{,i} - \mu^2\left(\frac{h}{2}(h\overline{u}_{j,jt})_{,i} - \frac{h^2}{6}(\overline{u}_{j,jt})_{,i}\right) = 0 \tag{121}$$

We further introduce the notation

$$H = h + \delta\eta = h + \delta(\eta_c + \eta_w) = H_c + \delta\eta_w. \tag{122}$$

Using (119) and (122) in (120)-(121) and using a suitable average over wave phase denoted by $\langle\rangle$, we obtain an equation for mass conservation for the mean flow given by

$$H_{c,t} + (H_c u_{cj} + \delta\langle\eta_w u_{wj}\rangle)_{,j} = 0, \tag{123}$$

where the wave averaged quantity is the wave-induced mass flux. Denoting the total mean flow velocity by

$$u_{ti} = u_{ci} + \frac{\delta}{H_c}\langle\eta_w u_{wi}\rangle, \tag{124}$$

we may further write the mean flow momentum equation as

$$(H_c u_{ti})_t + (H_c u_{ti}u_{tj})_{,j} + H_c\eta_{c,i} + \delta S_{ij,j} = O(\delta^2), \tag{125}$$

where dispersive effects on the slowly varying mean flow are simply dropped in lieu of a more thorough scaling argument. The tensor S_{ij} is the radiation stress tensor

$$S_{ij} = H_c\langle u_{wi}u_{wj}\rangle + \frac{1}{2}\langle\eta_w^2\rangle \tag{126}$$

and the term $S_{ij,j}$ provides the forcing to drive steady or low-frequency motions. Turning to the equations for the fluctuating motion, we return to vector notation and denote the wave-induced velocity as $\mathbf{u}_w$ and

current velocity as $\mathbf{u}_c$. The resulting governing equations are

$$\eta_{w,t} + \nabla \cdot [H\mathbf{u}_w + \delta\eta_w\mathbf{u}_c - \delta\langle\eta_w\mathbf{u}_w\rangle] = 0 \qquad (127)$$

$$\mathbf{u}_{wt} + \delta(\mathbf{u}_c + \mathbf{u}_w)\cdot\nabla\mathbf{u}_w + \delta\mathbf{u}_w\cdot\nabla\mathbf{u}_c + \nabla\eta_w - \frac{1}{3}\mu^2h^2\nabla(\nabla\cdot\mathbf{u}_{wt}) = 0, \qquad (128)$$

where we have further neglected bottom slope effects in the dispersive terms. The decomposition here is based on the assumption that the largest component of the mean flow is of the same order as the wave induced velocity; $\mathbf{u}_w = O(\delta\sqrt{gh})$ in dimensional form. However, it is occasionally the case (particularly in tidal inlets and estuarine entrances) that the mean flow velocity can become the same order of magnitude as the free wave speed $\sqrt{gh}$, and thus exceed the wave-induced orbital motion in size. This case is not adequately covered by the weakly-nonlinear Boussinesq models as given because it implies a fluid velocity which is larger than assumed in the initial perturbation analysis. Yoon and Liu [95] have considered this case in detail and have rederived the depth-averaged equations, including a separate large current from the start. The principle revisions to the resulting governing equations occur only in the dispersive terms for the wave motion, and essentially occur due to the advection of the dispersive wave motion by the large current. Equation (128) may be corrected to this more general level of approximation by replacing the $O(\mu^2)$ dispersive term by the expression

$$\frac{1}{3}\mu^2H_c^2\nabla\left[\nabla\cdot\mathbf{u}_{wt} + \mathbf{u}_c\cdot\nabla(\nabla\cdot\mathbf{u}_w)\right], \qquad (129)$$

which essentially replaces the local derivative in the original expression with a total derivative following the mean flow. The fully nonlinear Boussinesq models described in section 3 do not impose an absolute scaling on the size of velocity components, and thus contain Yoon & Liu's extension of the theory within the single set of model equations. These models are thus completely valid for the computation of wave motions on relatively large currents. The consistency of the model equation with the dispersive term (129) may be seen by constructing its linear dispersion relation, which reads (in dimensional form)

$$\sigma^2 = \frac{gk^2H_c}{1 + \frac{1}{3}(kH_c)^2}. \qquad (130)$$

where

$$\sigma = \omega - ku_c \qquad (131)$$

is the relative or intrinsic frequency. Equation (130) is a consistant approximation to the full linear dispersion relation for waves on a large current u_c.

Since the forcing for steady or low-frequency motion implied by (125) is embedded in the original Boussinesq or Serre model, computations involving wave breaking should generate longshore currents or other more complex nearshore circulation patterns directly. For the case of a periodic incident wave train, the steady wave-induced current can be extracted using a simple time average of the computational results. An example of such a current pattern may be found in Sørensen *et al* [96], who illustrate the computation of a rip current driven by longshore bathymetric variations on an otherwise straight coastline. A computed water surface and one half of the resulting circulation cell are shown in Figures 9 and 10.

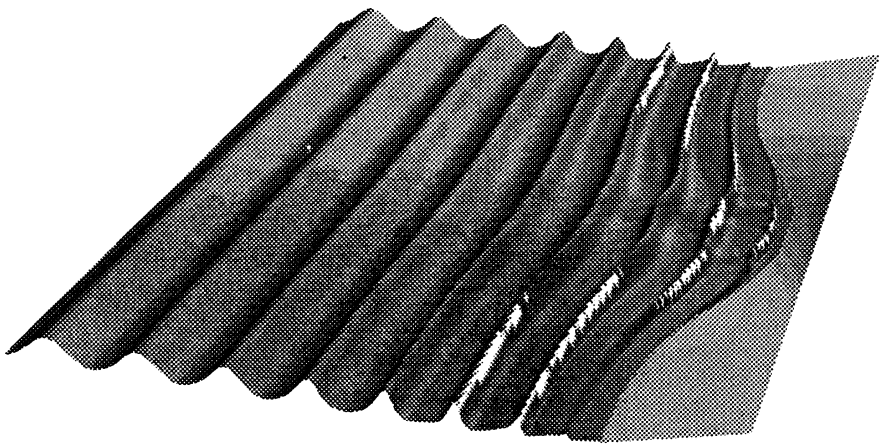

Figure 9: Birds-eye view of the free surface elevation for the rip channel case with regular waves. The surface rollers are shown in white. (from [96]).

9 Models for wave propagation with a principal direction

In addition to the models discussed above, which are all essentially fully two-dimensional in the horizontal plane (or have the capability to be extended in such a way), a considerable amount of work has been done on modelling schemes which involve the *a priori* choice of a preferred or principal propagation direction. These modelling schemes typically take the form of first-order wave equations in this principal direction, extended to include effects due to nonlinearity, frequency dispersion, weak transverse structure in the wave field and variations in the fluid domain in the propagation or transverse directions. This subject has also been recently reviewed by Akylas [97].

Historically, the first member of this class of models was developed by Korteweg and deVries [3] and is known as the Korteweg-deVries or KdV equation. For waves propagating in the $+x$-direction, the equation may be written in stationary coordinates as

$$\eta_t + \eta_x + \delta\frac{3}{2}\eta\eta_x + \mu^2\frac{1}{6}\eta_{xxx} = 0, \tag{132}$$

where the constant depth $h = h_0$ and where the linearized phase speed c normalized by $c_0 = \sqrt{gh_0}$ is given by

$$c = 1 - \frac{1}{6}\mu^2. \tag{133}$$

Note that the KdV equation exhibits the same kind of cutoff in prediction of a positive phase speed at high frequencies as seen in the Boussinesq equations based on velocity at the mean water level, although the problem of imaginary speeds and subsequent instability is avoided. This effect was addressed by Peregrine [77] and Benjamin *et al* [98], who introduced the model equation

$$\eta_t + \eta_x + \delta\frac{3}{2}\eta\eta_x - \mu^2\frac{1}{6}\eta_{xxt} = 0, \tag{134}$$

which has a corresponding linear phase speed

$$c = \frac{1}{1 + \frac{1}{6}\mu^2}, \tag{135}$$

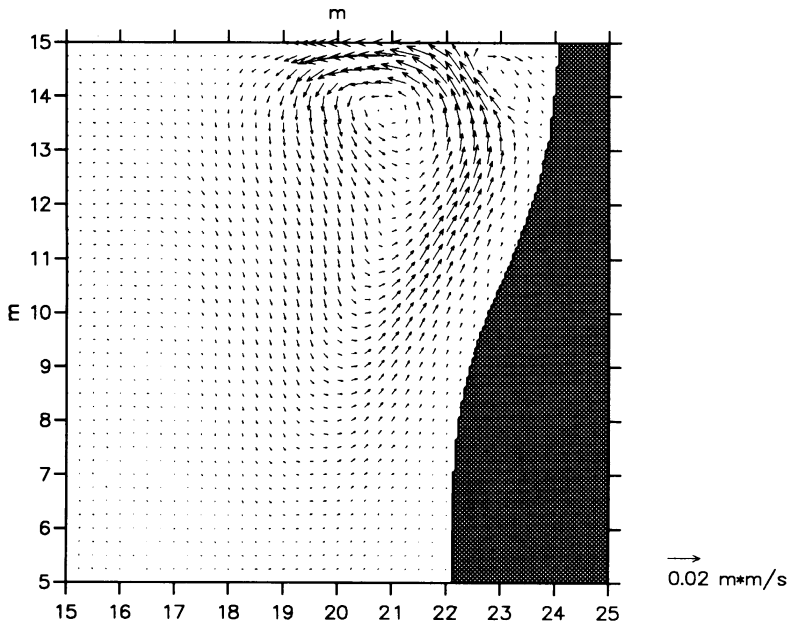

Figure 10: Depth-integrated velocity for the situation shown in Figure 9 focussing on a circulation cell (from [96]).

which is positive for all wave lengths. Equation (134) is commonly referred to as the BBM or Regularized Long Wave (RLW) equation.

For the case where a transverse y-direction structure in the wavefield is permitted (with characteristic y direction scales of $O(1/\mu)$ relative to x-direction scales), Kadomtsev and Petviashvili [99] introduced the perturbed KdV equation (now commonly referred to as the KP equation)

$$(\eta_t + \eta_x + \delta\frac{3}{2}\eta\eta_x + \mu^2\frac{1}{6}\eta_{xxx})_x + \mu^2\frac{1}{2}\eta_{YY} = 0, \qquad (136)$$

where $Y = \mu y$. As in the case of the KdV equation, the KP equation is also solvable by means of inverse scattering transforms and is thus the subject of considerable mathematical interest. There is also a solution describing families of biperiodic waves (i.e., periodic in both the x and y directions); see Segur and Finkel [100] and references therein. Hammack *et al* [101] [102] have studied the correspondence between these solutions and short crested nonlinear waves generated in a laboratory basin, and

have shown a close correspondence between model and data, and also that the theoretical restriction that the transverse lengthscale be large relative to the lengthscale in the propagation direction is not a strong restriction on applicability of the model equation.

In the following, we review recent efforts made in the direction of extending and applying these one-dimensional or weakly two-dimensional models to the problem of wave propagation in regions with varying depth.

9.1 Weakly two-dimensional propagation

The first KP equation for wave propagation in a variable domain with arbitrary depth $h(\mathbf{x})$ was given by Liu *et al* [103], who obtained it primarily from an examination of existing KP and variable-coefficient KdV models. Using a more formal perturbation expansion, Philip [104] suggested that a more appropriate form of the model can be written as

$$\left(\eta_t + c\eta_x + \delta c \frac{h_x}{4h}\eta + \delta \frac{3c}{2h}\eta\eta_x + \mu^2 \frac{ch^2}{6}\eta_{xxx} \right)_x + \mu^2 \frac{1}{2c}\left(c^2 \eta_Y\right)_Y = 0, \tag{137}$$

where c is dimensionless phase speed $c = (h/h_0)^{1/2}$, and where we assume that bottom slope in the propagation direction is $O(\delta)$. This equation is the same as the equation presented in [103] to within terms of $O(\mu^2)$ times the bottom slope, which is smaller than terms retained in the model equation. The model was used as the basis for constructing a parabolic approximation for forward-scattered waves [68], and was found to be an accurate predictor of wave focusing over variable bathymetry. Kirby *et al* [105] used this model to compute the Mach reflection of solitary waves from a vertical wall, and further extended the model coefficents to include the case of two-layer flow over topography. The form of the linearized, nondispersive model corresponding to (137) can also be justified using a splitting method applied to the usual linear long wave equation [105] [106]; this approach also provides the equation for the backward-propagating wave component as well as the coupling between the forward and backward modes due to linear reflection effects. A similar KP model has been developed by Chen [107].

A number of additional studies have provided KP models for a wide range of physical settings, including surface and internal waves with Coriolis-induced rotation [108] [109], gradually-varying channel width and background flow [110] [111]. Chen & Liu [113] have provided a

derivation of a comprehensive KP model covering all of these effects, with some restriction on the allowed variability of bottom topography.

In most of the studies mentioned above, the domain in which waves are propagating is assumed to be a channel with topography which varies very weakly in the transverse direction. The depth may then be written as

$$h(\mathbf{x}) = \tilde{h}(x) + \delta B(\mathbf{x}), \tag{138}$$

where it is assumed that deviations from the average depth in the transverse direction are $O(\delta)$ relative to the average depth. This assumption prompts a reformulation of the bottom boundary condition (6), which after expanding about the depth $\tilde{h}$ becomes

$$u\tilde{h}_x + \delta \mathbf{u} \cdot \nabla B = -w + \delta B w_z + O(\delta^2); \qquad z = -\tilde{h}(x). \tag{139}$$

This expansion has the effect of eliminating transverse depth variation effects in the leading order solutions for the dependent variables in the problem. The primary consequence of this is to remove the depth h from within the y derivative terms in (136) or (137). The resulting model for surface waves without background current [112] [113] may be written in the present notation as

$$\left(\eta_t + \tilde{c}\eta_x + \mu^2 \tilde{c}\frac{\tilde{h}_x}{4\tilde{h}}\eta + \frac{3\tilde{c}\delta}{2\tilde{h}}\eta\eta_x + \mu^2\frac{\tilde{c}\tilde{h}^2}{6}\eta_{xxx} + \delta\frac{\tilde{c}B}{2\tilde{h}}\eta_x\right)_x + \mu^2\frac{\tilde{c}}{2}\eta_{YY} = 0, \tag{140}$$

where $\tilde{c} = (\tilde{h}/h_0)^{1/2}$.

For simplicity, most studies to date have provided computational examples based on the assumption that channel sidewalls are impermeable vertical structures. Mathew & Akylas [114] provide an extension to the model system to account for sidewalls which are sloped in such a way as to still be confined to a region which is narrow compared to the main region of the channel, but which are sloped gradually enough to affect the dynamics of the motion in the channel.

Published tests of these model equations against actual data are lacking. The model (140) with the assumption of weak transverse dependence in the bottom topography has the advantage of being transformable into a standard KP equations for several topographies of interest [112], and thus analytic information on the deformation of solitary waves by this class of topographies is immediately available. It is the present author's feeling that models which invoke this restriction may be too restrictive for

application to general coastal topographies, although this is not known conclusively at present.

9.2 One-dimensional propagation

The assumption of one-dimensional propagation in long wave theory is quite restrictive. In open coastal applications, it implies a complete lack of directionality in the incident wave field. The results of various studies (to be discussed below) have indicated that results of one-dimensional model calculations, while not capable of reproducing the two-dimensional spatial geometry of the water surface, can give statistical measures which are consistent with point measurements to a remarkable degree. For the case of laterally unbounded motion (or for motion in a channel of constant width $2b$), Johnson [115] derived a variable depth KdV equation which may be written in stationary coordinates as [116]

$$\eta_t + c\eta_x + \delta\frac{c_x}{2}\eta + \delta\frac{3c}{2h}\eta\eta_x + \mu^2\frac{ch^2}{6}\eta_{xxx} = O(\delta^2, \delta\mu^2), \qquad (141)$$

where $h(x)$ is an arbitary function of x with a derivative of $O(\delta)$ in size, and where $c = (h/h_0)^{1/2}$ is the nondispersive phase speed scaled by a value based on the reference depth h_0. This equation may also be altered into the form of a RLW equation by changing the dispersive term. Svendsen and Hansen [117] sought to solve (141) for the case of cnoidal waves propagating over a gently sloping bottom by assuming the bottom slope to be an order smaller than indicated above, after which a first order solution to the equation gives the usual cnoidal wave as the local solution. The second order correction then produces an an antisymmetric perturbation about the wave crest, leading to a wave form which is pitched slightly forward at the crest. It is not clear how applicable an approach such as this would be to the problem of arbitary topography, since several phenomena of clear importance (such as the continued deformation of a shoaled wave over a shallow shelf) would not be reproduced. Most subsequent attention has been focused on purely computational approaches.

For waves propagating in laterally-bounded channels, motion becomes essentially one-dimensional if the horizontal lengthscale of the motion along the channel greatly exceeds the lengthscale characterizing the channel width. Peregrine [118] gave a method for constructing Boussinesq

equations for the case of a uniform channel of arbitrary cross-section, and transformed the resulting equations to a KdV equation as well. Teng & Wu [119] [120] have provided extensions of both a Boussinesq model and a KdV model to the case of a channel of arbitrary cross section which is allowed to vary along the channel length. For the case of a rectangular channel of depth $h(x)$ and half width $b(x)$, the KdV form of their model was given originally by Shuto [121] and may be written in the form

$$b\eta_t + bc\eta_x + \delta\frac{(bc)_x}{2}\eta + \delta\frac{3bc}{2h}\eta\eta_x + \mu^2\frac{bch^2}{6}\eta_{xxx} = 0. \qquad (142)$$

Miles [122] has pointed out that (142) is non-conservative of mass, with the mass conservation equation given by

$$\frac{d}{dt}\int_{x_0}^{\infty} b\eta dx = Q(x_0), \qquad (143)$$

where

$$Q(x_0) = \left(bc\eta + \delta\frac{3bcn^2}{4h} + \mu^2\frac{bch^2}{6}\eta_{xx}\right)|_{x=x_0} + \frac{1}{2}\int_{x_0}^{\infty}(bc)_x\eta dx. \qquad (144)$$

The first set of terms in brackets in (144) represents the flux of mass across a station $x = x_0$. Miles concludes that the integral term in (144) represents a transfer of mass to a reflected wave. Kirby & Vengayil [106] constructed coupled KdV equations for opposite going waves using a splitting technique, verified Miles' conclusion, and further established the two-way mechanism for mass transfer between the opposite going waves. Based on direct computations and comparison to experimental data [123], Kirby & Vengayil also concluded that the small additional terms that Miles used to rearrange the variable coefficient equation into its integral form should be include in the model system from the outset, giving a rectangular channel equation of the form

$$(b\eta^{\pm})_t \pm bc\eta^{\pm}_x + \delta\frac{(bc)_x}{2}(\eta^+ - \eta^-) \pm \left[\delta\frac{3bc(\eta^{\pm})^2}{4h} \mp \mu^2\frac{bh^2}{6}\eta^{\pm}_{xt}\right]_x = 0, \quad (145)$$

where $+(-)$ denotes rightward(leftward) propagating waves. Mattioli [124] has further extended these equations by including the nonlinear coupling between the right and left running waves.

10 Frequency domain formulations

The computation of a time dependent wave field as a means of simulating a complex field condition presents a numerical modeller with essentially the same problem as that faced by the experimentalist — how to interpret the physical implications of a flood of data. The most prevalent data analysis technique for either regular waves or statistically stationary random waves is Fourier analysis. It therefore makes some sense to consider a computation of the desired wave field in the frequency domain rather than the time domain, since most of the effects being looked for in the frequency domain are directly available from the computations without further analysis. This is especially true for shallow water waves, where the final stage of highly nonlinear wave evolution can be characterized by a rapid transfer of energy from the fundamental (or spectral peak in the case of random waves) to higher or lower harmonics, by means of nearly resonant three-wave interactions. Much of the original impetus for the development of these methods came from a study of the water wave analogy of the process of *second harmonic generation*, long known in nonlinear optics [125]. Mei & Ünlüata [126] and Boczar-Karakiewicz [127] studied the phenomenon of second harmonic generation and recurrence in weakly-dispersive long waves using the spectral approach, and showed that the method provided an accurate description of the phenomenon; see also [128] [129]

In this section, we review recent results obtained using spectral methods in the context of the variable depth problem.

10.1 Deterministic models in the frequency domain

Spectral equations for wave shoaling and evolution have been presented in a number of different formats and notations. In this section, we will present evolution equations for complex Fourier amplitude rather than separating the resulting equations into equations for real amplitude and phase.

In order to illustrate the structure of a deterministic model for water wave shoaling, we derive such a model from the variable depth KdV equation (141). We write the surface displacement η as a Fourier series

with amplitudes A_n, which are assumed to vary on a slow spatial scale $X = \delta x$ of the same order as variations in water depth;

$$\eta = \sum_{n=1}^{N} \left(\frac{A_n(X)}{2} \mathrm{e}^{i\psi_n} + \frac{A_n^*(X)}{2} \mathrm{e}^{-i\psi_n} \right), \tag{146}$$

where $()^*$ denotes a complex conjugation, and where the series is terminated at N components for computational reasons. The phase function ψ_n is given by

$$\psi(n)(x,t) = \frac{1}{\delta} \int_X k_n(X) dX - \omega_n t \tag{147}$$

and we assume that the wavenumber and frequency for each model are given by linear nondispersive theory at leading order; $\omega_n^2 = k_n^2 h$. We proceed by substituting (146) in (141), collecting terms of $O(\delta, \mu^2)$, and then isolating the contributions to the motion at each frequency component n. In this last step, we assume that the dominant mechanism leading to nonlinear interaction between different frequency components is resonant three wave interaction (see Phillips [130], Section 3.8). We thus ignore any contributions from quadratic terms which are not oscillating at the same frequency as the target frequency component n and obtain the set of evolution equations

$$\begin{aligned} &A_{n,X} + \frac{h_X}{4h} A_n - i \frac{\mu^2}{\delta} n^3 k \frac{(kh)^2}{6} A_n \\ &+ \frac{3ink}{8h} \left[\sum_{l=1}^{n-1} A_l A_{n-l} + 2 \sum_{l=1}^{N-n} A_l^* A_{n+l} \right] = 0, n = 1, ..., N. \end{aligned} \tag{148}$$

The resulting model equation gives the rate of change of the Fourier amplitude for each frequency component due to the leading-order effects of shoaling, frequency dispersion, and nonlinear interaction. This model was originally given by Vengayil & Kirby [131], who extended it to include laminar bottom friction effects and compared it to data for shoaling periodic waves [63]. It is also essentially equivalent to the 'consistent' model given by Freilich & Guza [132], and is so named because it retains only the leading order effect of each small term in the original model equation. Kirby [133] has shown that, for this level of truncation, the evolution equation being solved would actually be most analogous to a modified KdV equation of the form

$$\eta_t + \eta_x - \delta \frac{3}{2} \eta \eta_t - \mu^2 \frac{1}{6} \eta_{ttt} = 0, \tag{149}$$

which has higher wave phase speeds and broader solitary wave crests than corresponding solutions of the original KdV equations.

Systems of the form (148) may be applied to either regular or irregular wave. For the case of regular wave data, it is sufficient to compute the complex Fourier spectrum A_n for one period of the wave, and use this as input data to initialize the model at some station x. The equations are then solved by marching in x to obtain the complex Fourier spectrum at more shoreward locations, after which the time series may be reconstructed, if desired, using the inverse transform. For the case of irregular waves, the process used is essentially similar to the computation of smoothed power spectra from measurements. The time series of data is broken into a set of shorter series, each of which is transformed to give an ith realization of complex spectrum, A_n^i. The individual realizations are then used to initialize separate model runs. The results of computations at desired x locations are then collected and used to compute smoothed statistical estimates. For example, an estimate of the power spectrum $S_n = |A_n|^2/2$ based on I realizations of the data would be given by

$$S_n = \frac{1}{2I} \sum_{i=1}^{I} |A_n^i|^2. \tag{150}$$

This process can be somewhat painstaking, as the integration of (148) can become quite stiff and cause adaptive step size schemes to grind to a halt. Nevertheless, it is a reliable approach in most instances.

Freilich & Guza have shown that a model equivalent to (148) is capable of reproducing most of the features of spectral evolution during the random wave shoaling process, including amplification of the spectrum due to shoaling as well as the transfer of energy to higher harmonics of the spectral peak. The consistent model given here actually tends to overpredict purely linear shoaling effects due to the lowest-order representation of the shoaling process used. The shoaling term in (148) dictates that the amplitude of any one Fourier component evolves (in the absence of nonlinear effects) according to Green's Law

$$\left| \frac{A_n(x)}{A_n(x_0)} \right| = \left(\frac{h(x_0)}{h(x)} \right)^{1/4}, \tag{151}$$

which can cause serious overprediction of amplitude for components initialized at a sizeable depth. This problem is partially alleviated by retaining inhomogeneous domain effects arising from the dispersive terms.

Freilich & Guza presented a model which retained additional effects in both shoaling terms and nonlinear coupling coefficients; this model has been extensively tested against data and has been seen to be a robust predictor of second and third-moment statistics [134]– [137], even in cases where wave directional spreading becomes significant.

Madsen & Sørensen [129] have considered the modification of the Boussinesq model for the purpose of obtaining accurate shoaling coefficients in spectral models; see also [45]. However, since each frequency component is separately identified, it is in fact possible to represent full linear dispersive effects in the individual equations. Such an approach has been pursued by Agnon *et al* [138], who used the spectral Zhakharov equations to formulate a one-dimensional model, and by Kaihatu & Kirby [139], who developed a set of mild slope equations coupled at second-order in wave steepness and extended Agnon *et al* 's model to two horizontal dimensions.

For the case where directional spreading of waves becomes significant, it is necessary to move to a two-dimensional or weakly two-dimensional format. Liu *et al* [103] developed a two-dimensional spectral model in the form of a coupled set of parabolic models; this model is reviewed in [68]. In order to overcome the angular restrictions implied by the use of a parabolic approximation, Kirby [140] developed a model using a Fourier decomposition in both time and the longshore direction y. The model then steps a complex directional spectrum in the $+x$-direction. Several computational examples involving laboratory data are available for either of these models, but extensive testing against field data is lacking.

10.2 Bispectra and third moment statistics

As waves become significantly nonlinear during the shoaling process, they become asymmetric in both the vertical and horizontal directions. In terms of statistics, the vertical asymmetry is referred to as *skewness* and is given by the normalized third moment of the sea surface, while horizontal asymmetry is called *asymmetry* and is given most directly by the normalized third moment of the Hilbert transform of the sea surface. Both of these quantities are directly related to a third-order spectrum known as the *bispectrum*. A raw complex bispectral value is given in terms of complex Fourier amplitudes by

$$B_{i,j} = A_i A_j A^*_{i+j}. \tag{152}$$

The bispectrum plays a central role in the detection of nonlinearity in a random wave train, with the real part of the bispectrum related to the presence of in-phase harmonics (as in a regular periodic Stokes or cnoidal wave) and the imaginary part related to the presence of phase-locked but out-of-phase harmonics (as in a sawtooth waveform). In this guise, the real part presents the distribution of contributions to skewness over the frequency domain, while the imaginary part gives the distribution of contributions to asymmetry.

In the context of spectral models, the bispectrum has an immediate dynamical consequence. If we rearrange (148) into the form of an energy equation (by multiplying by A_n^* and adding A_n times the conjugate of (148)), we get the set of model equations

$$|A_n|_X^2 + \frac{h_X}{2h}|A_n|^2 = \frac{3n\delta}{4}\left[\sum_{l=1}^{n-1} \Im(B_{l,n-l}) + 2\sum_{l=1}^{N-n} \Im(B_{n,l}\right], \qquad (153)$$

where $\Im$ denotes the imaginary part. The presence of imaginary bispectral components is thus directly tied to the transfer of energy between spectral components. The characteristic pitched-forward sawtooth form of surf zone waves is representative of a rapid, sustained transfer of energy towards higher frequencies. This transfer must continue throughout the surf zone as long as the waves remain bore-like in nature. The cessation of breaking and reformation of a less asymmetric individual wave also implies a cessation of this energy transfer process. This result has consequences for the development of wave breaking models, which are considered next.

10.3 Wave breaking

The problem of modelling wave breaking in a spectral model is fraught with difficulties. The fact that dissipation mechanisms are highly localized in time (i.e., confined to the roller region as the roller advects past a fixed observer) indicates that they should have a global representation in the frequency domain, with all frequency components being mutually dependent. There is no existing model which includes these effects at this level of complexity. Instead, there has been a tendency to approach the problem by appending a dissipation term to the spectral model (148), giving a model of the form

$$A_{n,X} + \cdots = -\alpha_n A_n, \qquad (154)$$

The α_n are usually chosen by using a bulk energy decay model to compute the energy loss for the entire modelled spectrum, and then distributing this loss in some weighted manner across the frequency spectrum. An early attempt using this approach was made by Liu [141], who studied the breaking of regular periodic waves [63]. Liu chose to use a distribution of α_n's with no dependence on frequency. The resulting wave forms in the modelled surf zone show a marked lack of asymmetry, which is at odds with the known tendency for surf zone waves to become sawtoothed in form. Based on the arguments in the previous section, it is clear that this approach suppressed the transfer of energy from the fundamental to higher harmonics, indicating an over-accumulation of energy at relatively high frequency. Thus, though wave height and total variance are reasonably predicted, third moment predictions are essentially destroyed. This approach has also been followed in a recent application using random waves by Eldeberky & Battjes [142].

Mase & Kirby [83] considered the problem of the dependence of α_n on frequency. Based on observations of data for the breaking of a wave train characterized by a smooth, Pierson-Moskowitz spectrum, they concluded that α_n should have a quadratic dependence on frequency. Using this distribution, they were able to obtain accurate predictions of the evolution of wave heights, power spectra and higher moments for the simple spectral shapes considered.

Despite the indications of partial success observed so far, the accurate prediction of transformation and breaking of complex, multi-peaked spectra has still not been accomplished. It is likely that a successful model will need to retain some of the global nature of the dissipation process in the frequency domain, as mentioned above. Models of this type are under development but are undocumented at present.

10.4 Stochastic model formulations

The recent implementation of deep ocean or shelf scale wind wave models has depended to a large extent on the use of action flux models aimed at directly computing wave statistics as opposed to any phase-retaining deterministic portrait of the individual waves [143]. It is tempting to apply this approach in the nearshore wave environment as well, although the underlying assumption of random phases, which is central to the development of statistical closures in intermediate depth action flux models, is

hard to justify in shallow water applications, where the presence of rapid spectral energy transfer implies strong phase coupling between spectral components.

The framework for developing stochastic closures for spectral models is known from several fields. Equation (153) can be averaged over a number of realizations to yield a model for the smoothed power spectrum S_n which depends on the smoothed bispectrum. It is then necessary to construct a model to compute the evolution of the bispectrum based on values of the trispectrum, or fourth order spectral moments. This cascade extends to all orders, and hence a closure problem becomes apparent. Work in this format is in its infancy and will not be well documented for some time yet. There is some indication that the equations for the bispectra can be closed in terms of products of power spectral components. It is not clear that this closure will yield a simpler computational environment than the deterministic model described above, as the number of bispectral components essentially goes like N^2 and thus the number of equations needed to compute a broad spectrum will rival the number of solutions for multiple realizations needed in the deterministic framework.

There is one existing example in the literature of an attempt to invoke a simpler closure and thereby confine the number of equations to be solved to the number of spectral components. This is given by Abreu *et al* [144], who used a closure proposed by Newell & Aucoin [145] which is limited to strictly resonant interactions. The model formulation is quite restrictive in that it neglects all interactions between waves travelling in different directions, as is required by the limitation to tuned resonances. However, it is well known that there are directional interactions in spectral wave fields [146] [147]. Directional interactions are also crucial in the formation of hexagonal patterns in biperiodic wave structures and in the formation of Mach stems [140].

Despite these negative conclusions about the first attempted low-order closure scheme, it will continue to be highly desirable to develop approximate closures which eliminate part of the burden of computing the entire bispectrum in future stochastic models.

11 Future Directions

The maturation of the theoretical basis and numerical methods for the Boussinesq equations has led to a recent explosion of effort aimed at utilizing these models for coastal engineering prediction. A number of purely hydrodynamic models have been discussed above. Recently, models coupling the hydrodynamics to sediment transport models aimed at predicting seabed evolution have also been developed [148] [149]. Further development and testing in this area needs to be done.

The future is certain to see an extension of the Boussinesq and similar equations to $O(\mu^4)$ [150]. Since the present $O(\mu^2)$ models with corrected dispersive properties are capable of predicting the propagation of waves over most of the range of shoaling water depths, modifications of the model equations to include $O(\mu^4)$ effects are likely to provide a limited set of improvements if propagation characteristics are the primary concern. Indeed, there are no existing data sets which would adequately test the improved performance of an $O(\mu^4)$ propagation model. The main reason for providing such an extension to the theory would be to provide a more accurate predictive capability for the fluid kinematics, which are not as well predicted as the propagation characteristics are at present. Any model extension in this direction should be based closely on a related model of the fluid kinematics carried to comparable accuracy, in order to reap a significant benefit from the extension.

In the realm of spectral applications, the future is likely to hold the development of a number of stochastic models, in which the deterministic methods prevalent to date are replaced by methods for computing the wave power spectrum, together with higher spectral moments. As mentioned above, these methods are just now in their earliest stages of development.

Acknowledgement This review was made possible by support from the Army Research Office through University Research Initiative grant DAAL 03-92-G-0116. I also wish to thank Ge Wei, who assisted in the preparation of figures, and Tony Dalrymple and Tuba Özkan, who provided critical readings of the manuscript.

References

[1] Airy, Tides and waves, *Encycl. Metrop.*, 1845, Section VI.

[2] Boussinesq, J.V. Théorie des ondes et des remous qui se propagent le long d'un canal rectangulaire horizontal, en communiquant au liquide contenu dans ce canal des vitesses sensiblement pareilles de la surface au fond, *J. Math. Pures Appliq.*, 1872, **17**, 55-108. (An English translation of this article by A.C.J. Vastano & J.C.H. Mungall is available as Reference 76-2-T, Department of Oceanography, Texas A&M University, March 1976.)

[3] Korteweg, D.J. & de Vries, G. On the change of form of long waves advancing in a rectangular canal, and on a new type of long stationary waves, *Phil. Mag.* , 1895, **39**, 422-443.

[4] Gardner, C.S., Greene, J.M., Kruskal, M.D. & Miura, R.M. Method for solving the Korteweg-deVries equation, *Phys. Rev. Lett.*, 1967, **19**, 1095-1097.

[5] Lax, P.D. Integrals of nonlinear equations of evolution and solitary waves, *Comm. Pure & Appl. Math.*, 1968, **21**, 467-490.

[6] Dodd, R.K., Eilbeck, J.C., Gibbon, J.D. & Morris, H.C. *Solitons and nonlinear wave equations*, 1982, London, Academic Press.

[7] Drazin, P.G. & Johnson, R.S. *Solitons: an introduction*, 1989, Cambridge, Cambridge University Press.

[8] Mei, C.C. & Le Méhauté, B. Note on the equations of long waves over an uneven bottom, *J. Geophys. Res.*, 1966, **71**, 393-400.

[9] Peregrine, D.H. Long waves on a beach, *J. Fluid Mech.*, 1967, **27**, 815-827.

[10] Madsen, O.S. & Mei, C.C. The transformation of a solitary wave over an uneven bottom, *J. Fluid Mech.*, 1969, **39**, 781-791.

[11] Abbott, M.B., Petersen, H.M. & Skovgaard, O. On the numerical modelling of short waves in shallow water, *J. Hydr. Res.*, 1978, **16**, 173-204.

[12] Madsen, P.A. & Warren, I.R. Performance of a numerical short-wave model, *Coast. Engrng.*, 1984, **8**, 73-93.

[13] Rygg, O.B. Nonlinear refraction-diffraction of surface waves in intermediate and shallow water, *Coastal Engrng.*, 1988, **12**, 191-211.

[14] Luke, J.C. A variational principle for a fluid with a free surface, *J. Fluid Mech.*, 1967, **27**, 395-397.

[15] Miles, J.W. On Hamilton's principle for surface waves, *J. Fluid Mech.*, 1977, **83**, 153-158.

[16] Arnold, V.I. *Mathematical Methods of Classical Mechanics*, 1989, New York, Springer-Verlag.

[17] Zhakharov, V.E. Stability of periodic waves of finite amplitude on the surface of a deep fluid, *J. Appl. Mech. Tech. Phys.*, 1968, **9**, 190-194.

[18] Lemos, C.M. *Wave breaking: a numerical study*, 1992, Lecture Notes in Engineering 71, New York, Springer-Verlag.

[19] Dommermuth, D.G. & Yue, D.K.P. A high-order spectral method for the study of nonlinear gravity waves, *J. Fluid Mech.*, 1987, **184**, 267-288.

[20] West, B.J., Brueckner, K.A., Janda, R.S., Milder, D.M. & Milton, R.L. A new numerical method for surface hydrodynamics, *J. Geophys. Res.*, 1987, **92**, 11803-11824.

[21] Radder, A.C. An explicit Hamiltonian formulation of surface waves in water of finite depth, *J. Fluid Mech.*, 1992, **237**, 435-455.

[22] Otta, A.K. and Dingemans, M.W., Hamiltonian formulation of water waves, Report H 782, 1994, Delft Hydraulics.

[23] Grilli, S.T., Skourup, J. & Svendsen, I.A. An efficient boundary element method for nonlinear water waves, *Engrng. Anal. with Boundary Elements*, 1989, **6**, 97-107.

[24] Grilli, S.T. Modeling of nonlinear wave motion in shallow water. In *Computational methods for free and moving boundary problems in heat and fluid flow* (ed. L.C. Wrobel & C.A. Brebbia), 1993, Elsevier, pp. 37-65.

[25] Grilli, S.T., Subramanya, R., Svendsen, I.A. & Veeramony, J. Shoaling of solitary waves on plane beaches, *J. Waterway, Port, Coast. & Ocean Engrng.*, 1994, **120**, 609-628.

[26] Vinje, T. & Brevig, P. Numerical simulation of breaking waves, *Adv. Water Resources*, 1981, **4**, 77-82.

[27] Kim, S.K., Liu, P.L.F. & Liggett, J.A. Boundary integral equation solutions for solitary wave generation, propagation and runup, *Coast. Engrng.*, 1983, **7**, 299-317.

[28] Cointe, R. Numerical simulation of a wave channel, *Engrng. Anal. with Boundary Elements*, 1990, **7**, 167-177.

[29] Ohyama, T. & Nadaoka, K. Transformation of a nonlinear wave train passing over a submerged shelf without breaking, *Coast. Engrng.*, 1994, **24**, 1-22.

[30] Romate, J.E. The numerical simulation of nonlinear gravity waves in three dimensions using a higher order panel method, Thesis, Techn. Univ. Twente, 1989.

[31] Broeze,J. Numerical modelling of nonlinear free surface waves with a 3D panel method, Thesis, Techn. Univ. Twente, 1993.

[32] Mei, C.C. *The applied dynamics of ocean surface waves*, 1989, Singapore, World Scientific.

[33] Serre, F. Contribution à l'étude des écoulements permanents et variables dans les canaux, *La Houille Blanche*, 1953, **3**, 374-388 and 830-872.

[34] Su, C.H. & Gardner, C.S. Korteweg-deVries equation and generalizations. III. Derivation of the Korteweg-deVries equation and Burgers equation, *J. Math. Phys.*, 1969, **10**, 536-539.

[35] Green, A.E. & Naghdi, P.M. A derivation of equations for wave propagation in water of variable depth, *J. Fluid Mech.*, 1976, **78**, 237-246.

[36] Witting, J.M. A unified model for the evolution of nonlinear water waves, *J. Comp. Phys.*, 1984, **56**, 203-236.

[37] Nwogu, O. Alternative form of Boussinesq equations for nearshore wave propagation, *J. Waterway, Port, Coast. and Ocean Engrng.*, 1993, **119**, 618-638.

[38] Madsen, P.A., Murray, R. & Sorensen, O.R. A new form of the Boussinesq equations with improved linear dispersion characteristics, *Coastal Engrng.*, 1991, **15**, 371-388.

[39] Madsen, P.A. & Sorensen, O.R. A new form of the Boussinesq equations with improved linear dispersion characteristics. Part 2. A slowly-varying bathymetry, *Coastal Engrng.*, 1992, **18**, 183-204.

[40] McCowan, A.D. & Blackman, D.R. The extension of Boussinesq-type equations to modelling short waves in deep water, *Proc. 9th Australasian Conf. Coast. Ocean Engrng.*, Adelaide, 1989, 412-416.

[41] Nadaoka, K., Beji, S. & Nakagawa, Y. A fully-dispersive nonlinear wave model and its numerical solutions, *Proc. 24th Intl. Conf. Coast. Engrng.*, Kobe, 1994, 427-441.

[42] Wu, T.Y. Long waves in ocean and coastal waters, *J. Engineering Mech.*, 1981, **107**, 501-522.

[43] Wei, G., Kirby, J.T., Grilli, S.T. & Subramanya, R. A fully nonlinear Boussinesq model for surface waves. I. Highly nonlinear, unsteady waves, *J. Fluid Mech.*, 1995, **294**, 71-92.

[44] Chen, Y. & Liu, P.L.F. Modified Boussinesq equations and associated parabolic models for water wave propagation, *J. Fluid Mech.*, 1995, **288**, 351-381.

[45] Dingemans, M.W. Water wave propagation over uneven bottoms, Dissertation, Delft University of Technology, 1994.

[46] Broer, L.J.F. On the Hamiltonian theory of surface waves, *Appl. Sci. Res.*, 1974, **30**, 430-446.

[47] Broer, L.J.F. Approximate equations for long water waves, *Appl. Sci. Res.*, 1975, **31**, 377-395.

[48] Broer, L.J.F., van Groesen, E.W.C. & Timmers, J.M.W. Stable model equations for long water waves, *Appl. Sci. Res.*, 1976, **32**, 619-636.

[49] Katapodes, N.D. & Dingemans, M.W. Stable equations for surface wave propagation on an uneven bottom, 1988, Delft Hydraulics.

[50] Mooiman, J. Boussinesq equations based on a positive definite Hamiltonian, Report Z294, 1991, Delft Hydraulics.

[51] Van der Veen, W.A. & Wubs, F.W. A Hamiltonian approach to fairly low and fairly long gravity waves. *Report W-9314, Department of Mathematics, Univ. of Groningen*, 1993.

[52] Yoon, S.B. & Liu, P.L.F. A note on Hamiltonian for long water waves in vaying depth, *Wave Motion*, 1994, **20**, 359-370.

[53] Tanaka, M. The stability of solitary waves, *Phys. Fluids*, 1986, **29**, 650-655.

[54] Seabra-Santos, F.J., Renouard, D.P. & Temperville, A.M. Numerical and experimental study of the transformation of a solitary wave over a shelf or isolated obstacle, *J. Fluid Mech.*, 1987, 117-134.

[55] Wei, G. & Kirby, J.T. A coastal processes model based on time-domain Boussinesq equations, Report *CACR-96-01*, Center for Applied Coastal Research, University of Delaware. Paper presented at *Coastal Dynamics '95*, Gdansk, September 4-8, 1995.

[56] Green, A.E., Laws, N. & Naghdi, P.M. On the theory of water waves, *Proc. Roy. Soc. A*, 1974, **338**, 43-55.

[57] Miles, J.W. & Salmon, R. Weakly dispersive nonlinear gravity waves, *J. Fluid Mech.*, 1985, **157**, 519-531.

[58] Ertekin, R.C., Webster, W.C. & Wehausen, J.V. Waves caused by a moving disturbance in a shallow channel of finite width, *J. Fluid Mech.*, 1986, **169**, 275-292.

[59] Shields, J.J. & Webster, W.C. On direct methods in water-wave theory, *J. Fluid Mech.*, 1988, **197**, 171-199.

[60] Shields, J.J. & Webster, W.C. Conservation of mechanical energy and circulation in the theory of inviscid fluid sheets, *J. Engrng. Math.*, 1989, **23**, 1-15.

[61] Demirbilek, Z. & Webster, W.C. Application of the Green-Naghdi theory of fluid sheets to shallow water wave problems, Technical Report CERC-92-11, U.S. Army Corps of Engineers, Vicksburg, MS, 1992.

[62] Shields, J.J. A direct theory for waves approaching a beach, Ph. D. Dissertation, University of California at Berkeley, 1986.

[63] Hansen, J.B. & Svendsen, I.A. Regular waves in shoaling water, experimental data, Series Paper 21, ISVA, Techn. Univ. Denmark, 1979.

[64] Demirbilek, Z. & Webster, W.C. Users manual and examples for GN-WAVE, Technical Report CERC-92-13, U.S. Army Corps of Engineers, Vicksburg, MS, 1992, 55 pp.

[65] Webster, W.C. & Wehausen, J.V. Bragg scattering of water waves by Green-Naghdi theory, *Z. angew Math. Phys.*, 1995, **46** Special issue, S566-S583.

[66] Dingemans, M.W. Comparison of computations with Boussinesq-like models and laboratory measurements, Report H1684.12, 1994, Delft Hydraulics.

[67] Berkhoff, J.C.W., Booij, N. & Radder, A.C. Verification of numerical wave propagation models for simple harmonic linear water waves, *Coastal Engineering*, 1982, **6**, 255-279.

[68] Martin, P.A., Dalrymple, R.A. & Kirby, J.T. Parabolic modelling of water waves, 1996, present volume.

[69] Kirby, J.T. & Dalrymple, R.A. Verification of a parabolic equation for propagation of weakly-nonlinear waves, *Coastal Engrng.*, 1984, **8**, 219-232.

[70] Wei, G. & Kirby, J.T. Time-dependent numerical code for extended Boussinesq equations, *J. Waterway, Port, Coast. and Ocean Engrng.*, 1995, **121**, 251-261.

[71] Mooiman, J. Comparison between measurements and a Boussinesq model for wave deformation by a shoal, Report Z294, Part II, 1991, Delft Hydraulics.

[72] Hibberd, S. & Peregrine, D.H. Surf and runup on a beach: a uniform bore, *J. Fluid Mech.*, 1979, **95**, 323-345.

[73] Packwood, A.R. & Peregrine, D.H. The propagation of solitary waves and bores over a porous bed, *Coastal Engrng.*, 1980, **3**, 221-242.

[74] Kobayashi, N., DeSilva, G.S. & Watson, K.D. Wave transformation and swash oscillation on gentle and steep slopes, *J. Geophys. Res.*, 1989, **94**, 951-966.

[75] Kobayashi, N. & Wurjanto, A. Irregular wave setup and runup on beaches, *J. Waterway, Port, Coast. & Ocean Engrng.*, 1992, **118**, 235-251.

[76] Raubenheimer, B., Guza, R.T., Elgar, S. & Kobayashi, N. Swash on a gently sloping beach, *J. Geophys. Res.*, 1995, **100**, 8751-8760.

[77] Peregrine, D.H. Calculations of the development of an undular bore, *J. Fluid Mech.*, 1966, **25**, 321-330.

[78] Karambas, Th., Krestenitis, Y. & Koutitas, C. A numerical solution of Boussinesq equations in the inshore zone, *Hydrosoft*, 1990, **3**, 34-37.

[79] Karambas, Th.V. & Koutitas, C. A breaking wave propagation model based on the Boussinesq equations, *Coastal Engrng.*, 1992, **18**, 1-19.

[80] Zelt, J.A. The run-up of nonbreaking and breaking solitary waves, *Coastal Engnrng.*, 1991, **15**, 205-246.

[81] Heitner, K.L. & Housner, G.W. Numerical model for tsunami runup, *J. Waterway, Port, Coast. & Ocean Engrng.*, 1970, **96**, 701-719.

[82] Synolakis, C.E. The run-up of long waves, Ph. D. thesis, Calif. Inst. Technol., 1986.

[83] Mase, H. & Kirby, J.T. Hybrid frequency-domain KdV equation for random wave transformation, *Proc. 23d Intl. Conf. Coastal Engrng.*, 1992, Venice, 474-487,

[84] Svendsen, I.A. Wave heights and setup in a surf zone, *Coast. Engrng.*, 1984, **8**, 303-329.

[85] Deigaard, R. Mathematical modelling of waves in the surfzone, Progr. Report 69, ISVA, Technical Univ. Denmark., 1989, 47-59.

[86] Schäffer, H.A., Madsen, P.A. & Deigaard, R. A Boussinesq model for waves breaking in shallow water, *Coastal Engnrng.*, 1993, **20**, 185-202.

[87] Madsen, P.A., Sorensen, O.R. & Schäffer, H.A. Time domain modelling of wave breaking, runup, and surf beats, *Proc. 24th Intl. Conf. Coast. Engrng.*, Kobe, 1994, 399-411.

[88] Brocchini, M., Drago, M. & Iovenitti, L. The modelling of short waves in shallow waters. Comparison of numerical models based on Boussinesq and Serre equations, *Proc. 23d Intl. Conf. Coast. Engrng.*, Venice, 1992, 76-88.

[89] Pedersen, G. & Gjevik, B. Run-up of solitary waves, *J. Fluid Mech.*, 1983, **135**, 283-299.

[90] Özkan, H.T. & Kirby, J.T. Finite amplitude shear wave instabilities, *Proc. Coastal Dynamics '95*, Gdansk, 1995, 465-476.

[91] Carrier, G.F. & Greenspan, H.P. Water waves of finite amplitude on a sloping beach, *J. Fluid Mech.*, 1958, **4**, 97-109.

[92] Liu, P.L.F., Cho, Y.S., Briggs, M.J., Kanoglu, U. & Synolakis, C.E. Runup of solitary waves on a circular island, *J. Fluid Mech.*, 1995, **302**, 259-285.

[93] Tao, J. Computation of wave run-up and wave breaking, Internal Report, Danish Hydraulic Institute, 1983.

[94] Casulli, V. & Cheng, R.T. Semi-implicit finite difference methods for three-dimensional shallow water flow, *Intl. J. Numer. Meth. Fluids*, 1992, **15**, 629-648.

[95] Yoon, S.B. & Liu, P.L.F. Interactions of currents and weakly nonlinear water waves in shallow water, *J. Fluid Mech.*, 1989, **205**, 397-419.

[96] Sørensen, O.R., Schäffer, H.A., Madsen, P.A. & Deigaard, R. Wave breaking and induced nearshore circulations, *Proc. 24th Intl. Conf. Coast. Engrng.*, Kobe, 2583-2594.

[97] Akylas, T.R. Three-dimensional long water-wave phenomena, *Ann. Rev. Fluid Mech.*, 1994, **26**, 191-210.

[98] Benjamin, T.B., Bona, J.L. & Mahoney, J.J. Model equations for long waves in nonlinear dispersive systems, *Phil. Trans. Roy. Soc. A*, 1972, **272**, 47-78.

[99] Kadomtsev, B.B. & Petviashvili, V.I. On the stability of solitary waves in weakly dispersing media, *Sov. Phys. Dokl.*, 1970, **15**, 539-541.

[100] Segur, H. & Finkel, A. An analytical model of periodic waves in shallow water, *Stud. Appl. Math.*, 1985, **73**, 183-220.

[101] Hammack, J.L., Scheffner, N. & Segur, H. Two-dimensional periodic waves in shallow water, *J. Fluid Mech.*, 1989, **209**, 567-589.

[102] Hammack, J.L., McCallister, D., Scheffner, N. & Segur, H. Two-dimensional periodic waves in shallow water. Part 2. Asymmetric waves, *J. Fluid Mech.*, 1995, **285**, 95-122.

[103] Liu, P.L.F., Yoon, S.B. & Kirby, J.T. Nonlinear refraction-diffraction of waves in shallow water, *J. Fluid Mech.*, 1985, **153**, 184-201.

[104] Philip, R. Numerical simulation of shallow water waves, M.S. thesis, University of Florida, 1988.

[105] Kirby, J.T., Philip, R. & Vengayil, P. One-dimensional and weakly two-dimensional waves in varying channels: numerical examples, in *Nonlinear water waves. Proc. IUTAM Symp. Tokyo 1987* (eds) K. Horikawa & H. Maruo, Springer Verlag, 1988, 357-364.

[106] Kirby, J.T. & Vengayil, P. Nonresonant and resonant reflection of long waves in varying channels, *J. Geophys. Res.*, 1988, **93**, 10782-10796.

[107] Chen, X.N. Unified Kadomtsev-Petviashvili equation, *Phys. Fluids A.* 1989, **1**, 2058-2060.

[108] Grimshaw, R. Evolution equations for weakly nonlinear, long internal waves in a rotating fluid, *Stud. Appl. Math.*, 1985, **73**, 1-33.

[109] Katsis, C. & Akylas, T.R. Solitary internal waves in a rotating channel: a numerical study, *Phys. Fluids*, 1987, **30**, 297-301.

[110] David, D., Levi, D. & Winternitz, P. Integrable nonlinear equations for water waves in straits of varying width and depth, *Stud. Appl. Math*, 1987, **76**, 133-168.

[111] David, D., Levi, D. & Winternitz, P. Solitons in shallow seas of variable depth and in marine straits, *Stud. Appl. Math*, 1989, **80**, 1-23.

[112] Iizuka, T. & Wadati, M. Shallow water waves over an uneven bottom and an inhomogeneous KP equation, *Chaos, solitons & fractals*, 1992, **2**, 575-582.

[113] Chen, Y. & Liu, P.L.F. The unified Kadomtsev-Petviashvili equation for interfacial waves, *J. Fluid Mech.*, 1995, **288**, 383-408.

[114] Mathew, J. & Akylas, T.R., On three-dimensional long water waves in a channel with sloping sidewalls, *J. Fluid Mech.*, 1990, **215**, 289-307.

[115] Johnson, R.S. On the development of a solitary wave moving over an uneven bottom, *Proc. Camb. Phil. Soc.*, 1973, **73**, 183-203.

[116] Svendsen, I.A. A direct derivation of the KdV equation for waves on a beach, and discussion of its implication, *ISVA Progr. Rept., Tech. Univ. Denmark*, 1976, **39**, 9-16.

[117] Svendsen, I.A. & Hansen, J.B. On the deformation of periodic long waves over a gently sloping bottom, *J. Fluid Mech.*, 1978, **87**, 433-448.

[118] Peregrine, D.H. Long waves in a uniform channel with arbitrary cross-section, *J. Fluid Mech.*, 1968, **32**, 353-365.

[119] Teng, M.H. & Wu, T.Y. Nonlinear water waves in channels of arbitrary shape, *J. Fluid Mech.*, 1992, **242**, 211-233.

[120] Teng, M. H. & Wu, T. Y. Evolution of long water waves in variable channels, *J. Fluid Mech.*, 1994, **266**, 303-317.

[121] Shuto, N. Nonlinear long waves in a channel of variable section, *Coast. Engrng. Japan*, 1974, **17**, 1-12.

[122] Miles, J.W. On the Korteweg-deVries equation for a gradually varying channel, *J. Fluid Mech.*, 1979, **91**, 181-190.

[123] Chang, P., Melville, W.K. & Miles, J.W. On the evolution of a solitary wave in a gradually varying channel, *J. Fluid Mech.*, 1979, **95**, 401-414.

[124] Mattioli, F. Decomposition of the Boussinesq equations for shallow-water waves into a set of couples Korteweg-deVries equations, *Phys. Fluids A*. 1991, **3**, 2355-2359.

[125] Armstrong, J.A., Bloembergen, N., Ducuing, J. & Pershan, P.S. Interactions between light waves in a nonlinear dielectric, *Phys. Rev.*, 1962, **127**, 1918-1939.

[126] Mei, C.C. & Ünlüata, Ü. Harmonic generation in shallow water waves. In *Waves on Beaches*, (ed) R.E. Meyer, 1972, New York Academic, pp. 181-202.

[127] Boczar-Karakiewicz, B. Transformation of wave profile in shallow water - a Fourier analysis, *Arch. Hydrotechniki*, 1972, **19**, 197-210.

[128] Chapalain, G., Cointe, R. & Temperville, A. Observed and modeled resonantly interacting progressive water waves, *Coast. Engrng.*, 1992, **16**, 267-300.

[129] Madsen, P.A. & Sørensen, O.R. Bound waves and triad interactions in shallow water, *Ocean Engrng.*, 1993, **20**, 359-388.

[130] Phillips, O.M. *The dynamics of the upper ocean*, 1977, Cambridge, Cambridge Univ. Press.

[131] Vengayil, P. & Kirby, J.T. Shoaling and reflection of nonlinear shallow water waves, *Proc. 20th Intl. Conf. Coasta. Engrng.*, Taipei, 1986, 794-806.

[132] Freilich, M.H. & Guza, R.T. Nonlinear effects on shoaling surface gravity waves, *Phil. Trans. R. Soc. London, Ser. A*, 1984, **311**, 1-41.

[133] Kirby, J.T. Intercomparison of truncated series solutions for shallow water waves, *J. Waterway, Port, Coast. and Ocean Engrng.*, 1991, **117**, 143-155.

[134] Elgar, S. & Guza, R.T. Shoaling gravity waves: comparisons between field observations, linear theory, and a nonlinear model, *J. Fluid Mech.*, 1985, **158**, 47-70.

[135] Elgar, S. & Guza, R.T. Observations of bispectra of shoaling surface gravity waves, *J. Fluid Mech.*, 1985, **161**, 425-448.

[136] Elgar, S. & Guza, R.T. Nonlinear model predictions of bispectra of shoaling surface gravity waves, *J. Fluid Mech.*, 1986, **167**, 1-18.

[137] Elgar, S., Freilich, M.H. & Guza, R.T. Model-data comparisons of moments of nonbreaking shoaling surface gravity waves, *J. Geophys. Res.*, 1990, **95**, 16055-16063.

[138] Agnon, Y., Sheremet, A., Gonsalves, J. & Stiassnie, M. Nonlinear evolution of a unidirectional shoaling wave field, *Coast. Eng.*, 1993, **20**, 29-58.

[139] Kaihatu, J.M. & Kirby, J.T. Nonlinear transformation of waves in finite water depth, *Phys. Fluids*, 1995, **7**, 1903-1914.

[140] Kirby, J.T. Modelling shoaling directional wave spectra in shallow water, *Proc. 22nd Intl. Conf. Coast. Engrng*, 1990, Delft, 109-122.

[141] Liu, P.L.F. Wave transformation, in *The Sea. Ocean Engineering Science, Volume 9, Part A*, (eds) B. Le Mehaute & D.M. Hanes, 1990, New York, Wiley, pp. 27-63.

[142] Eldeberky, Y. & Battjes, J.A. Spectral modeling of wave breaking: application to Boussinesq equations, *J. Geophys. Res.*, 1996, **101**, 1253-1264.

[143] Komean, G.J., Cavaleri, L., Donelan, M., Hasselmann, K., Hasselmann, S. & Janssen, P.A.E.M. *Dynamics and modelling of ocean waves*, 1994, Cambridge, Cambridge Univ. Press.

[144] Abreu, M., Larraza, A. & Thornton, E. Nonlinear transformation of directional wave spectra in shallow water, *J. Geophys. Res.*, 1992, **97**, 15579-15589.

[145] Newell, A.C. & Aucoin, P.J. Semidispersive wave systems, *J. Fluid Mech.*, 1971, **49**, 593-609.

[146] Freilich, M. H., Guza, R.T. & Elgar, S. Observations of nonlinear effects in directional spectra of shoaling gravity waves, *J. Geophys. Res.*, 1990, **95**, 9645-9656.

[147] Elgar, S., Guza, R.T. & Freilich, M.H. Observations of nonlinear interactions in directionally spread shoaling surface gravity waves, *J. Geophys. Res.*, 1993, **98**, 20,299-20,305.

[148] Mayerle, R., Schröter, A. & Zielke, W. Simulation of nearshore wave current interaction by coupling a Boussinesq wave model with a 3d hydrodynamic model, *Proc. 24th Intl. Conf. Coast. Engrng*, Kobe, 1994, 2340-2349.

[149] Sato, S. & Kabiling, M.B. A numerical simulation of beach evolution based on a nonlinear dispersive wave-current model, *Proc. 24th Intl. Conf. Coast. Engrng*, Kobe, 1994, 2557-2570.

[150] Schäffer, H.A. & Madsen, P.A. Further enhancements of Boussinesq-type equations, *Coastal Engineering*, 1995, **26**, 1-14.